

Science

March 2013, Volume 339 Issue 6125 Pages 1305-1308

<http://dx.doi.org/10.1126/science.1229240><http://archimer.ifremer.fr/doc/00176/28767/>

© 2013, American Association for the Advancement of Science

Achimer<http://archimer.ifremer.fr>

Evidence for Microbial Carbon and Sulfur Cycling in Deeply Buried Ridge Flank Basalt

Lever Mark A.^{1,2,*}, Rouxel Olivier^{3,4}, Alt Jeffrey C.⁵, Shimizu Nobumichi³, Ono Shuhei⁶,
 Coggon Rosalind M.⁷, Shanks Wayne C., Iii⁸, Lapham Laura², Elvert Marcus^{9,10},
 Prieto-Mollar Xavier^{9,10}, Hinrichs Kai-Uwe^{9,10}, Inagaki Fumio¹¹, Teske Andreas¹

¹ Univ N Carolina, Dept Marine Sci, Chapel Hill, NC 27599 USA.² Aarhus Univ, Dept Biosci, Ctr Geomicrobiol, DK-8000 Aarhus C, Denmark.³ Woods Hole Oceanog Inst, Woods Hole, MA 02543 USA.⁴ IFREMER, Ctr Brest, F-29280 Plouzane, France.⁵ Univ Michigan, Dept Earth & Environm Sci, Ann Arbor, MI 48109 USA.⁶ MIT, Dept Earth Atmospher & Planetary Sci, Cambridge, MA 02139 USA.⁷ Univ London Imperial Coll Sci Technol & Med, Dept Earth Sci & Engn, London SW7 2AZ, England.⁸ US Geol Survey, Denver, CO 80225 USA.⁹ Univ Bremen, Dept Geosci, Organ Geochem Grp, D-28334 Bremen, Germany.¹⁰ Univ Bremen, MARUM Ctr Marine Environm Sci, D-28334 Bremen, Germany.¹¹ Japan Agcy Marine Earth Sci & Technol, Kochi Inst Core Sample Res, Geomicrobiol Grp, Nanko Ku, Kochi 7838502, Japan.* Corresponding author : email address : mark.lever@biology.au.dk ; teske@email.unc.edu**Abstract :**

Sediment-covered basalt on the flanks of mid-ocean ridges constitutes most of Earth's oceanic crust, but the composition and metabolic function of its microbial ecosystem are largely unknown. By drilling into 3.5-million-year-old seafloor basalt, we demonstrated the presence of methane- and sulfur-cycling microbes on the eastern flank of the Juan de Fuca Ridge. Depth horizons with functional genes indicative of methane-cycling and sulfate-reducing microorganisms are enriched in solid-phase sulfur and total organic carbon, host $\delta^{13}\text{C}$ - and $\delta^{34}\text{S}$ -isotopic values with a biological imprint, and show clear signs of microbial activity when incubated in the laboratory. Downcore changes in carbon and sulfur cycling show discrete geochemical intervals with chemoautotrophic $\delta^{13}\text{C}$ signatures locally attenuated by heterotrophic metabolism.

Main text

Subseafloor basaltic crust represents the largest habitable zone by volume on Earth (1). Chemical reactions of basalt with seawater flowing through fractures release energy that may support chemosynthetic communities. Microbes exploiting these reactions are known from basalt exposed at the seafloor, where the oxidation of reduced sulfur (S) and iron (Fe) from basalt with dissolved oxygen and nitrate from seawater supports high microbial biomass and diversity (2, 3). Multiple lines of indirect evidence that include textural alterations (4), depletions in $\delta^{34}\text{S}$ -pyrite (FeS_2) (5) and $\delta^{13}\text{C}$ -dissolved inorganic carbon (DIC) (6), and DNA sequences from

51 borehole observatories (7, 8) suggest active microbial communities in subseafloor
52 basalt.

53 We combined sequencing of genes diagnostic of microbial methane- and S-
54 cycling with geochemical and isotopic analyses of C- and S-pools and laboratory-
55 based incubations to directly identify microbial ecosystem components in deep
56 subseafloor basalt. The 3.5 million-year-old basement at site U1301 was sampled
57 during Integrated Ocean Drilling Program (IODP) Expedition 301 in 2004 (Fig. S1)
58 (9). Site U1301 off the eastern flank of the Juan de Fuca ridge, is covered by a 265-m
59 thick sediment layer and lies ~2 km south of ODP Site 1026, which it resembles in
60 temperature profile, lithology, and sediment chemistry (9). Given anticipated poor
61 recovery due to brecciation of the upper basement (265-350 meters below seafloor;
62 mbsf), coring was restricted to an interval of pillow basalts and massive lavas (351-
63 583 mbsf). Sulfate concentrations (~16mM) and vein carbonates indicate basalt fluids
64 are derived from seawater, which enters ~80 km south at Grizzly Bare outcrop and
65 discharges near U1301, at Baby Bare and Mama Bare outcrops (9, 10; Fig. S1B). Yet,
66 the basement at U1301 differs from seafloor-exposed basalt in its uniformly high
67 temperature (~64°C) (9) and lack of fresh photosynthesis-derived organic matter,
68 dissolved oxygen and nitrate (7, 11). These conditions preclude oxygen- or nitrate-
69 dependent microbial S- and Fe-oxidation (12), but may enable growth of anaerobes,
70 such as sulfate reducers and methanogens, which use sulfate and DIC as electron
71 acceptors.

72 We sequenced genes encoding the α subunit of methyl coenzyme M reductase
73 (*mcrA*), a gene unique to methanogens and anaerobic methane-oxidizers (13), and the
74 β subunit of dissimilatory sulfite reductase (*dsrB*), a gene found in sulfate- and
75 sulfite-reducing microbes (14), to indicate the presence of methane-cycling and
76 sulfate-reducing microbes. We detect *mcrA* in 5 of the 10 samples and *dsrB* in 4 of the

77 6 samples tested (Table S1), suggesting that these metabolisms are present in this
78 environment.

79 The phylogenetic diversity of *mcrA* genes we identified is restricted to two
80 groups: the Juan de Fuca Methanogen Group (JdFMG), which falls into an
81 uncultivated cluster within the *Methanosarcinales*, and anaerobic methane-oxidizing
82 archaea (ANME-1; Fig. 1A). Close relatives of the JdFMG have been identified from
83 paddy and wetland soil (15, 16), and have also been found in marine habitats,
84 including Juan de Fuca Ridge hydrothermal vent chimneys and seafloor-exposed
85 basalt ~100 km west of U1301 (Fig. S2) (17, 18). ANME-1 occur widely in marine
86 sediments and methane seeps, and are believed to gain energy from the anaerobic
87 oxidation of methane (AOM) (19). Two distinct ANME phylotypes occur at U1301,
88 one closely related to ANME-1 from methane seeps, and another clustering with only
89 one other sequence, from subseafloor sediment (Fig. S3). We detected JdFMG in 4,
90 and ANME-1 in 3 out of 10 basalt samples. Two samples contained both groups
91 (Table S1).

92 The phylogenetic diversity of *dsrB* in these samples is limited to one group, the
93 Juan de Fuca Sulfate Reducing Group (JdFSRG), which falls into Cluster IV, a
94 deeply-branching *dsrB* cluster without cultured members, first reported from
95 hydrothermal sediment (Fig. 1B and S4, Table S1) (20). Remarkably, the only other
96 *dsr* sequences reported so far from the subseafloor – in sediment of the Peru Margin
97 (21) – also fall into this cluster, which is widespread in shallow marine sediment and
98 terrestrial aquifers.

99 We studied solid-phase S-pools by analyzing acid-volatile sulfide (AVS),
100 chromium-reducible S (CRS), and sulfate-S (SO₄-S) as a proxy to redox processes
101 and correlate to microbial metabolisms (5, 22). We only found *dsrB* sequences in a

102 relatively reduced ‘intermediate depth interval’ (~430-520 mbsf, 14R-26R), in
103 samples with AVS as the main S pool in alteration halos (14R-1-11) – the visually
104 conspicuous zone surrounding fractures (Fig. S1C) - or in host rock (17R-170, 20R-1-
105 57, 23R-2-21; Fig. S5, Table S1). Samples from this interval have higher AVS, CRS,
106 and total S (Fig. S5, Table S2), contain large pyrite fronts (14R-1-65P, 15R-4-142P;
107 Fig. S5), and have lower $\delta^{34}\text{S}$ -AVS, -CRS, and - $\text{SO}_4\text{-S}$, compared to the more
108 oxidized upper (1R-12R) and lower coring intervals (30R-36R; Fig. S6, Table S1).
109 Consistent with higher $\text{Fe}^{3+}/\text{Fe}^{\text{Total}}$ ratios, which indicate halos to be more oxidized
110 than host rock (Table S1), pyrite is generally absent from halos or veins. Outside the
111 intermediate depth interval, the near absence of pyrite from host rock, and mixed
112 clay-Fe-oxyhydroxide-dominated halos and veins are further evidence of pervasive
113 oxidative alteration.

114 We analyzed the $\delta^{34}\text{S}$ signature of pyrite grains to examine micro- and
115 macroscale variations in microbial S-cycling (Tables S1 and S3, Fig. 2). Though
116 variable, the $\delta^{34}\text{S}$ -pyrite grains (-72.4 to 1.2‰; Table S3) are typically lower than
117 those of AVS (-9.3 to -0.2‰), CRS (-13.7 to 0‰), $\text{SO}_4\text{-S}$ (-6.5 to 0‰), mantle S
118 (0‰) (5), dissolved sulfate in bottom sediments at ODP Site 1026 (+30‰) (23), or
119 seawater (+21‰; Fig. 2). Locally, the $\delta^{34}\text{S}$ of pyrite grains reach very negative values
120 (-72‰), consistent with the addition of highly ^{34}S -depleted secondary sulfide to
121 basement rock (22). These low $\delta^{34}\text{S}$ -pyrite values indicate single-step sulfate
122 reduction (24) or repeated cycles of sulfate reduction and S oxidation (25). The co-
123 occurrence of low $\delta^{34}\text{S}$ -pyrite, *dsrB*, and *mcrA* of ANME-1 in two samples (14R-1-
124 11, 17R-1-70) suggests local coupling between methane and S-cycling by sulfate-
125 dependent AOM.

126 Depth profiles of total organic carbon (TOC) content, $\delta^{13}\text{C}$ -TOC, and $\delta^{13}\text{C}$ -
127 carbonate at U1301B are consistent with functional gene- and ^{34}S -data (Fig. 3). The

128 TOC content is highest in the intermediate depth interval in cores with *mcrA*, *dsrB*,
129 and low $\delta^{34}\text{S}$ -pyrite (Fig. 3A, Table S4). The $\delta^{13}\text{C}$ -TOC is in the range of dissolved
130 organic C (DOC) in fluids from nearby 1026B and Baby Bare Springs (BBS; Fig. 3B,
131 Table S4) and lower than seawater DOC (-21.1‰; 6). The $\delta^{13}\text{C}$ -carbonate is higher
132 than $\delta^{13}\text{C}$ -DIC at 1026B or BBS (Fig. 3C, Table S5) and overlaps with $\delta^{13}\text{C}$ -DIC of
133 bottom seawater (-1.4‰; 10).

134 $\delta^{13}\text{C}$ -TOC values in the upper coring interval (4R-5R) and near the bottom
135 (23R-26R; -34.6 to -32.0‰) are close to $\delta^{13}\text{C}$ -DOC from nearby BBS (-34.6‰; Fig.
136 3B). The absence of O_2 and the high ^{13}C -TOC depletion relative to carbonate (~ -30
137 to -35‰) suggest C fixation by the reductive acetyl CoA pathway – an anaerobic
138 pathway found in all methanogens and acetogens, and certain sulfate and iron
139 reducers (Fig. S7, Tables S6 and S7; 26). The presence of *dsrB* but not *mcrA* in these
140 samples suggests that sulfate reducers or other groups, but not methanogens, produce
141 this low $\delta^{13}\text{C}$ -TOC.

142 $\delta^{13}\text{C}$ -TOC at the top (2R) and in the intermediate depth interval (-28.4 to -
143 21.6‰) are close to $\delta^{13}\text{C}$ -DOC from borehole 1026B (-26.1‰, Fig. 3B; 6). The ^{13}C -
144 depletion relative to carbonate is lower than in the other layers (~ -20 to -26‰), but
145 also falls in the range of the reductive acetyl CoA pathway (Table S7), and, consistent
146 with *mcrA* detection, could be impacted by autotrophic methanogenesis. In addition,
147 elevated heterotrophic activity is possible, since degradation of chemoautotrophy-
148 derived OC, e.g. by AOM, methanogenesis or fermentation, would lower the $\delta^{13}\text{C}$ -
149 carbonate and potentially raise the $\delta^{13}\text{C}$ -TOC. In fact, the lowest $\delta^{13}\text{C}$ -carbonate
150 values (to -5.1‰) were measured in the intermediate depth interval (18R; Fig. 3,
151 Table S5), consistent with a locally significant input of IC from the degradation of
152 chemoautotrophy-derived OC. The alternative explanation, enhanced breakdown of
153 photosynthesis-derived OC in the intermediate depth interval, is unlikely given that

154 sediment inclusions are absent (9). Similarly, influx of labile DOC or unaltered DIC
155 from seawater is incompatible with the 7-11 kyr greater DOC age compared to bottom
156 seawater and the 4-8‰ decrease in $\delta^{13}\text{C}$ -DIC along the flowpath from Grizzly Bare
157 outcrop to 1026B and BBS, respectively (6, 10).

158

159 To rule out a fossil origin of functional genes and the chemical and isotopic
160 signatures, we incubated pieces from the interior of three rock samples used for
161 functional gene analyses (1R-1-79, 14R-1-11, 23R-2-21) at 65°C in anoxic, sulfate-
162 rich media containing H_2 , acetate, methanol, and dimethyl sulfide as energy substrates
163 (Table S8). After two years, aliquots were transferred to fresh media, and incubated
164 for another five years using triple-autoclaved basalt pieces as substrata. By then, low
165 concentrations of ^{13}C -depleted methane (-54 to -65‰) had formed indicating the
166 presence of active methanogenic microorganisms (Table S9).

167

168 The variability in $\delta^{34}\text{S}$ -pyrite, $\delta^{13}\text{C}$ -TOC and $\delta^{13}\text{C}$ -carbonate indicates that
169 micro- and macro-scale geochemical changes related to mineralogy, fracturing and/or
170 fluid flow strongly influence microbial activity. These chemical microniches may
171 explain the coexistence of sulfate reducers and methanogens at U1301 and in other
172 igneous habitats, despite higher energy yields of sulfate reduction compared to
173 methanogenesis (27). In addition, some methanogens can survive in the presence of
174 sulfate reducers by consuming non-competitive methylated substrates (28). Since
175 methanogenic substrate usage follows *mcrA* phylogeny (28), this explanation is
176 consistent with the ability of a close relative of JdFMG to use methanol (16); it is also
177 consistent with the production of biogenic methane in basalt incubations containing
178 sulfate and methanol (Table S9, Fig. S8).

179 Inorganic electron donors used by sulfate reducers and methanogens, e.g. H_2 ,
180 are likely to derive from serpentinization reactions, whereby Fe(II) minerals, e.g.

181 olivine ((Mg, Fe)₂SiO₄), which is abundant in several basalt horizons at U1301 (9,
182 Fig. S9, Tables S10, S11), are oxidized in abiotic reactions with seawater-derived
183 fluids (1). Organic electron donors, e.g. short-chain fatty acids and alcohols, are
184 probably produced by breakdown of autochthonous OC (6, 27, 29) or Fischer-
185 Tropsch-type synthesis (30, Table S10). Targeted investigations of potential carbon
186 and energy sources will provide further insights to micro- and macroscale
187 heterogeneity of microbial C- and S-cycling, and thus contribute to a better
188 understanding of chemoautotrophic ecosystems within Earth's oceanic crust.

189

190 **References**

- 191 1. W. Bach, K. J. Edwards, *Geochim. Cosmochim. Acta* **67**, 3871 (2003).
- 192 2. K. J. Edwards, T. M. McCollom, H. Konishi, P. R. Buseck. *Geochim.*
193 *Cosmochim. Acta* **67**, 2843 (2003).
- 194 3. C. M. Santelli *et al.*, *Nature* **453**, 653 (2008).
- 195 4. M. R. Fisk, S. J. Giovannoni, I. H. Thorseth, *Science* **281**, 978 (1998).
- 196 5. O. Rouxel, S. Ono, J. Alt, D. Rumble, J. Ludden, *Earth Planet. Sci. Lett.* **268**,
197 110 (2008).
- 198 6. M. D. McCarthy *et al.*, *Nature Geosci* **4**, 32 (2011).
- 199 7. J. P. Cowen *et al.*, *Science* **299**, 120 (2003).
- 200 8. B. N. Orcutt *et al.*, *ISME J.* **5**, 692 (2011)
- 201 9. A. T. Fisher, T. Urabe, A. Klaus, Expedition 301 Scientists, *Proc. IODP 301*
202 (2005).
- 203 10. B. D. Walker, M. D. McCarthy, A. T. Fisher, T. P. Guilderson, *Mar. Chem.*
204 **108**, 123 (2008).
- 205 11. C. G. Wheat *et al.*, *Geochem. Geophys. Geosyst.* **11**, 1 (2010).
- 206 12. A. Schippers, B. B. Jørgensen, *Geochim. Cosmochim. Acta* **66**, 85 (2002).

- 207 13. M. W. Friedrich, *Meth. Enzymol.* **397**, 428 (2005).
- 208 14. M. Wagner, A. J. Roger, J. L. Flax, G. A. Brusseau, D. A. Stahl, *Appl.*
209 *Environ Microbiol.* **75**, 7086 (1998).
- 210 15. T. Lueders, K.-J. Chin, R. Conrad, M. Friedrich, *Environ. Microbiol.* **3**, 194
211 (2001).
- 212 16. G. Zhang *et al.*, *Environ. Microbiol.* **10**, 1850 (2008).
- 213 17. F. Wang *et al.*, *Proc. Nat. Acad. Sci. U.S.A.* **106**, 4840 (2009).
- 214 18. O. U. Mason *et al.*, *ISME J.* **3**, 231 (2009).
- 215 19. K. Knittel, A. Boetius, *Ann. Rev. Microbiol.* **63**, 311 (2009).
- 216 20. A. Dhillon, A. Teske, J. Dillon, D. A. Stahl, M. L. Sogin, *Appl. Environ.*
217 *Microbiol.* **69**, 2765 (2003).
- 218 21. G. Webster *et al.*, *FEMS Microbiol. Ecol.* **58**, 65 (2006).
- 219 22. S. Ono, N.S. Keller, O. Rouxel, J. C. Alt, *Geochim. Cosmochim. Acta* **87**, 323
220 (2012).
- 221 23. M. D. Rudnicki, H. Elderfield, B. Spiro, *Geochim. Cosmochim. Acta* **65**, 777
222 (2001).
- 223 24. M. S. Sim, T. Bosak, S. Ono, *Science* **333**, 74 (2011).
- 224 25. D. E. Canfield, B. Thamdrup, *Science* **266**, 1973 (1994).
- 225 26. A. L. Zerkle, C. H. House, S. L. Brantley, *Am. J. Sci.* 305, 467 (2005).
- 226 27. H.-T. Lin, J. P. Cowen, E. J. Olson, J. P. Amend, M. D. Lilley, *Geochim.*
227 *Cosmochim. Acta* **85**, 213 (2012).
- 228 28. W. B. Whitman, T. L. Bowen, D. R. Boone, *The Prokaryotes* **3**, 165 (2006).
- 229 29. M. A. Lever, *et al.*, *Geomicrobiol. J.* **27**, 183 (2010).
- 230 30. T. M. McCollom, J. S. Seewald, *Chem. Rev.* **107**, 382 (2007).
- 231
- 232 Supplementary online material references:
- 233 31. M. A. Lever *et al.*, *Geomicrobiol. J.* **23**, 517 (2006).
- 234 32. J. F. Biddle *et al.*, *Proc. Nat. Acad. Sci. U.S.A.* **103**, 3846 (2006).

- 235 33. M. A. Lever, Ph.D. Dissertation. University of North Carolina at Chapel Hill,
236 Chapel Hill, NC (2008).
- 237 34. W. Ludwig *et al.*, *Nucleic Acids Res.* **32**, 1363 (2004).
- 238 35. E. M. Ripley *et al.*, *Rev. Mineral. Geochem.* **73**, 9 (2011).
- 239 36. P. Craddock, O. Rouxel, L. Ball, W. Bach, *Chem. Geol.* **253**, 102 (2008).
- 240 37. A. Delacour, G. L. Früh-Green, S. M. Bernasconi, P. Schaeffer, D. S. Kelley,
241 *Geochim. Cosmochim. Acta* **72**, 3681 (2008).
- 242 38. B. N. Popp, F. J. Sansone, T. M. Rust, D. A. Merritt, *Anal. Chem.* **67**, 405
243 (1995).
- 244 39. C. H. House, J. W. Schopf, K. O. Stetter, *Org. Geochem.* **34**, 345 (2003).
- 245 40. S. Sakata, J. M. Hayes, M. Rohmer, A. B. Hooper, M. Seemann, *Org.*
246 *Geochem.* **39**, 1725 (2008).
- 247 41. M. Könneke, J. S. Lipp, K.-U. Hinrichs, *Org. Geochem.* **48**, 21 (2012).
- 248 42. K. L. Londry, D. J. Des Marais, *Appl. Environ. Microbiol.* **69**, 2942 (2003).
- 249 43. K. L. Londry, L. L. Jahnke, D. J. Des Marais, *Appl. Environ. Microbiol.* **70**,
250 745 (2004).
- 251 44. M. J. Alperin, T. M. Hoehler, *Am. J. Sci.* **309**, 958 (2009).
- 252 45. A. Gittel, K. B. Sørensen, T. L. Skovhus, K. Ingvorsen, A. Schramm, *Appl.*
253 *Environ. Microbiol.* **75**, 7086 (2009).
- 254 46. B. O. Steinsbu *et al.*, *Int. J. Syst. Evol. Microbiol.* **60**, 2745 (2010).

255

256 **Acknowledgments.** We thank B. Jørgensen, M. Sogin and the IODP Expedition 301
257 Scientists for advice and support in this project. Funding was obtained from a
258 Schlanger Ocean Drilling Fellowship, a University of North Carolina Dissertation
259 Completion Fellowship, a Marie-Curie Intra-European Fellowship (#255135; all to M.
260 Lever), the Danish National Research Foundation, the Max Planck Society (both to B.
261 Jørgensen), Europole Mer (to O. Rouxel), the European Research Council Advanced
262 Grant DARCLIFE (to K.-U. Hinrichs), the NASA Astrobiology Institute Subsurface

263 Biospheres (to A. Teske), the Japan Society for the Promotion of Science
264 (JSPS) Funding Program for Next Generation World-Leading Researchers (NEXT
265 Program; to F. Inagaki), and the National Science Foundation (NSF-OCE 0622949
266 and OCE 1129631 to J. Alt, OCE-0753126 to S. Ono and O. Rouxel, and NSF-ODP
267 0727175 and NSF-STC for Dark Energy Biosphere Investigations to A. Teske). We
268 thank three anonymous reviewers for very helpful comments. The geochemical data
269 are available in the Supplementary Tables. Experimental procedures are described in
270 Supplementary Online Materials. The functional gene sequence data are available
271 from Genbank database (accession numbers GU182109 to GU182110, and JX465656
272 to JX465658).

273 **FIGURES**

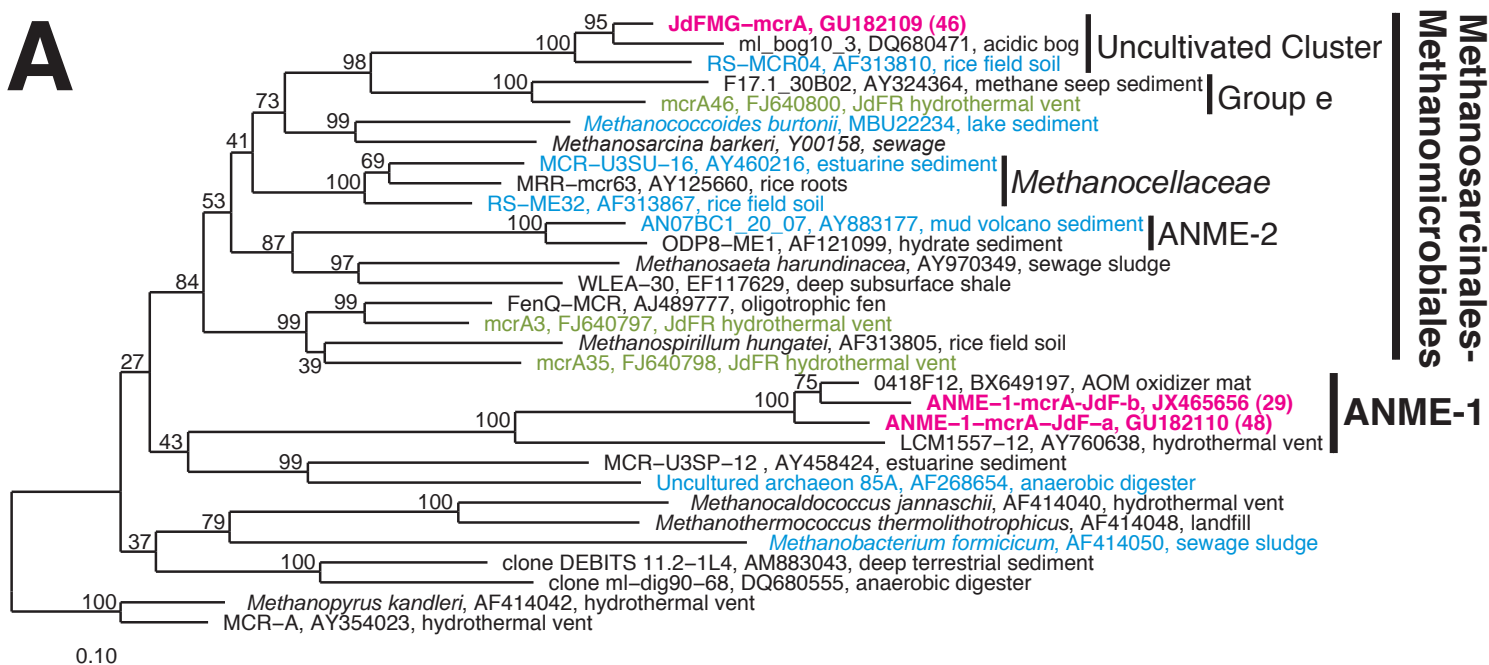
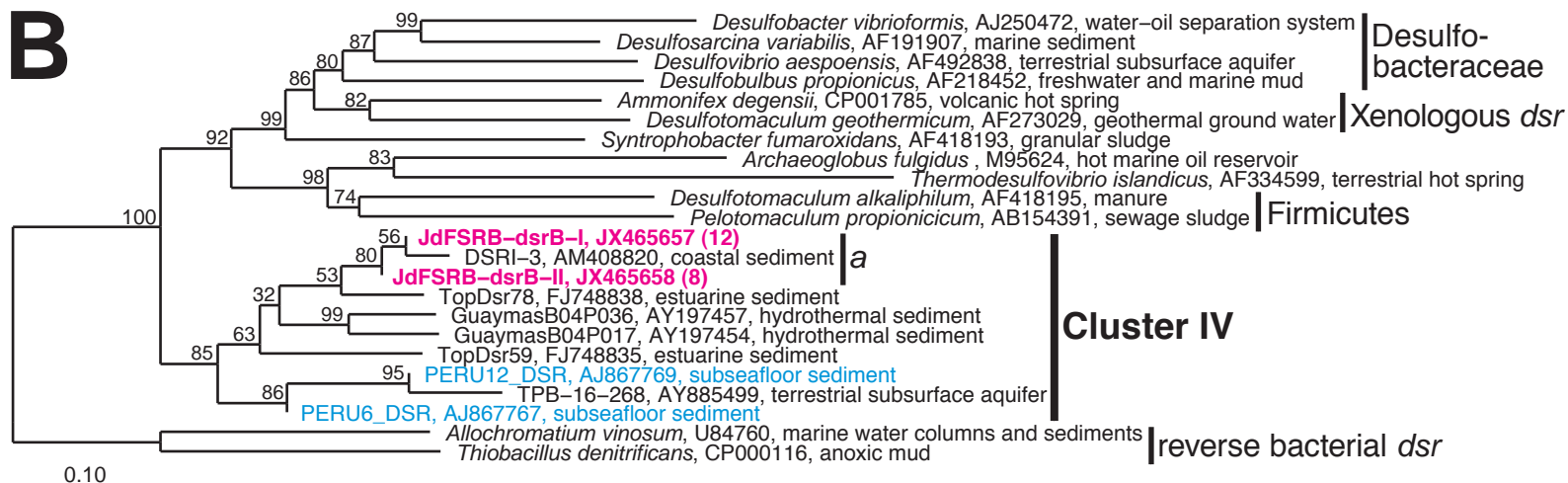
274 **Figure 1.** Phylogenetic trees of functional genes. (A) *McrA* sequences from borehole
 275 U1301B are in bold magenta type face. Close relatives based on microarray analyses
 276 of JdF Ridge hydrothermal vent chimneys and seafloor basalt are in green (18) and
 277 cyan (19), respectively. (B) *DsrB* sequences from borehole U1301B are in bold
 278 magenta type face, and sequences from subseafloor sediment off Peru in cyan (22).
 279 Bootstrap support (in %, 1,000 replications) is indicated at each branching point.

280

281 **Figure 2.** Macro- and micro-scale distribution of S-isotopic data. On the left, $\delta^{34}\text{S}$ -
 282 depth profile of pyrite granules, analyzed by laser ablation and secondary ion mass
 283 spectrometry (SIMS), and bulk S pools (AVS, CRS). On the right, thin section
 284 micrograph showing individual pyrite granules and their $\delta^{34}\text{S}$. The dashed magenta
 285 line indicates the sampling depth of the thin section. The dashed black lines mark the
 286 intermediate depth interval. Pyrite grains with a sufficient diameter for $\delta^{34}\text{S}$ -
 287 determination (10 μm) were limited to this interval. The scale bar is 200 μm .

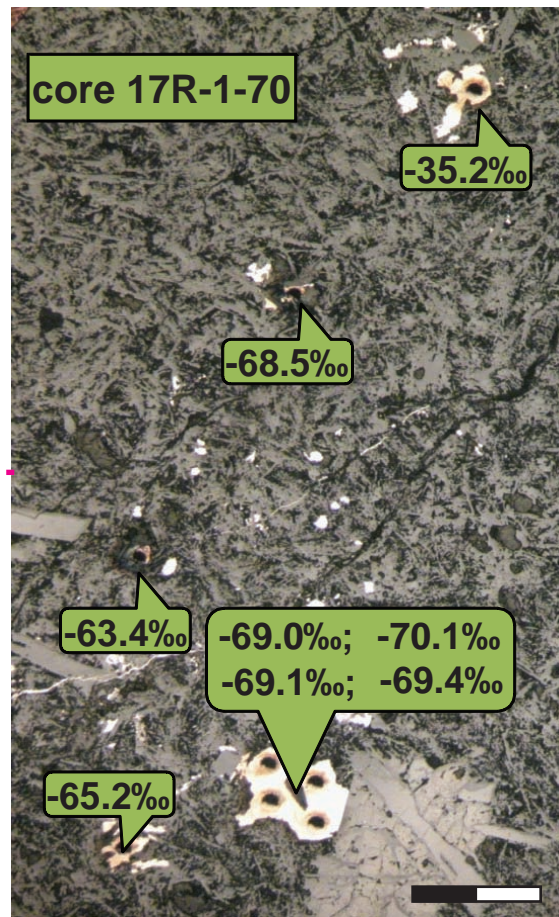
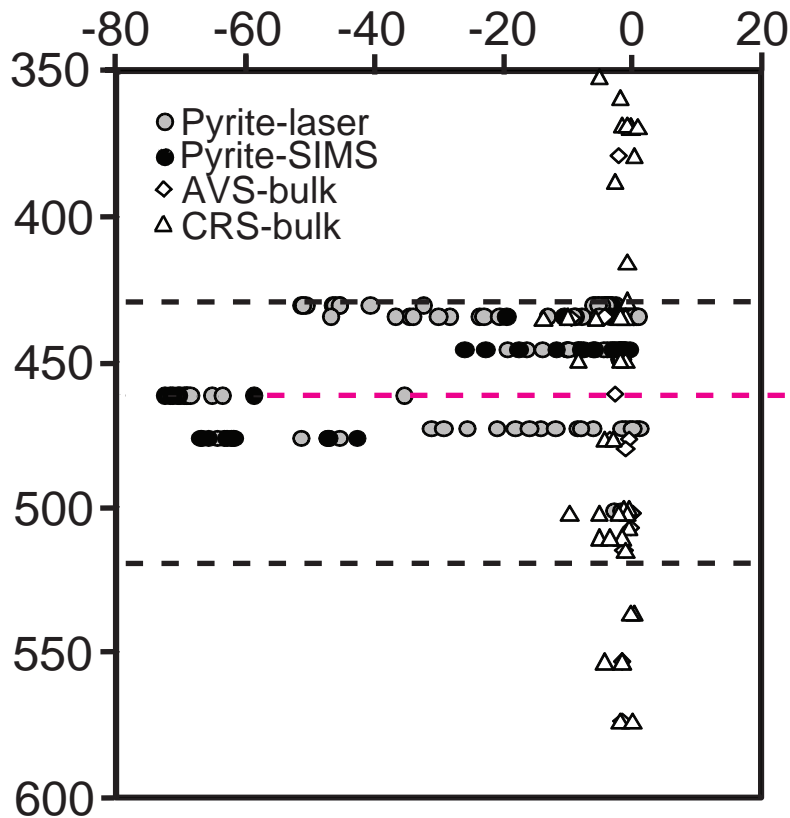
288

289 **Figure 3.** Depth-related trends in (A) TOC content, (B) $\delta^{13}\text{C}$ -TOC, and (C) $\delta^{13}\text{C}$ -
 290 carbonate. Cores with functional gene detection are indicated in A and B. Dashed
 291 vertical lines indicate $\delta^{13}\text{C}$ -DOC (B) and $\delta^{13}\text{C}$ -DIC (C) values from 1026B and BBS.
 292 Because the carbonate content of rock samples used in (A) and (B) was too low for
 293 analyses, $\delta^{13}\text{C}$ from carbonate veins are shown in (C). The reduced intermediate depth
 294 interval falls between the dashed horizontal lines. All $\delta^{13}\text{C}$ are in ‰ vs. VPDB.

A**B**

$\delta^{34}\text{S}$ (‰)

Depth (mbsf)



TOC (wt%)

$\delta^{13}\text{C}$ -TOC (‰)

$\delta^{13}\text{C}$ -carbonate (‰)

0.00 0.02 0.04 0.06 0.08 0.10

-36 -32 -28 -24 -20

-10 -8 -6 -4 -2 0 2

350

400

450

500

550

600

mcrA

mcrA, dsrB

mcrA, dsrB

dsrB

A

BBS

1026B

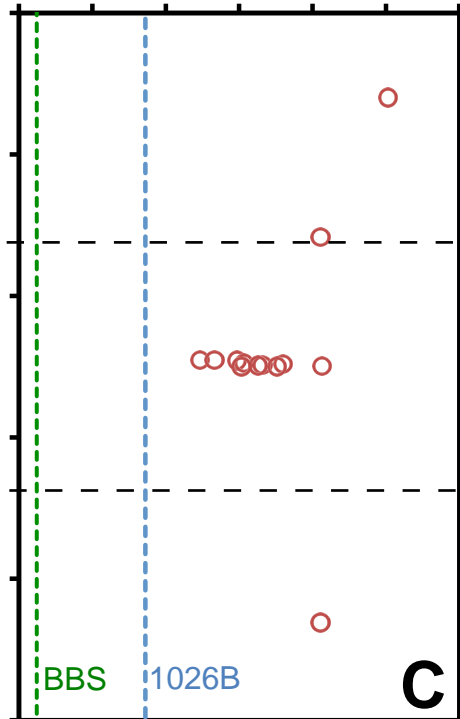
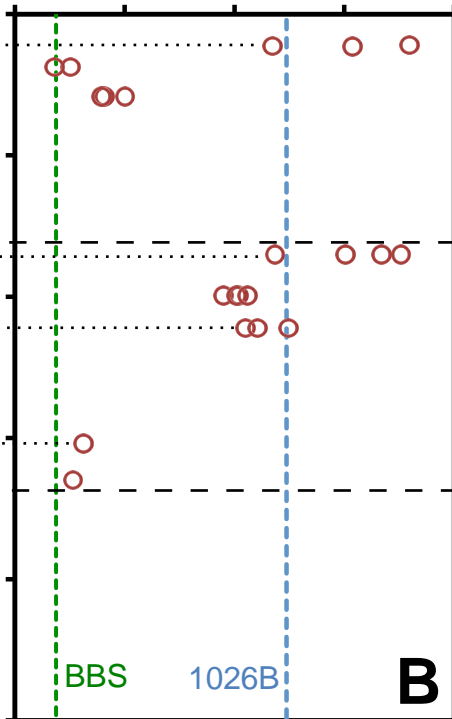
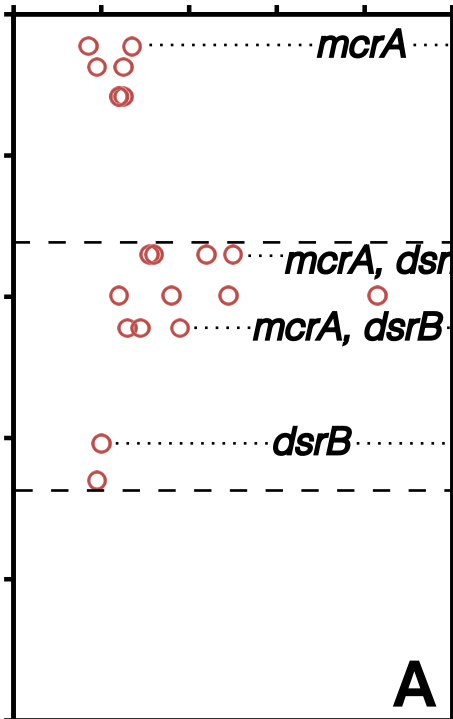
B

BBS

1026B

C

Depth (mbsf)



Supplementary Materials

Materials and Methods

Sample collection. Basalt cores from borehole U1301B were sampled using a Rotary Core Barrel (RCB) (9). Freshly recovered, intact whole-round basalt cores were decontaminated, cracked aseptically, and subsampled to measure drilling fluid contamination (31). For DNA extractions, only rock samples were used in which drilling fluid contamination was minimal (<2 contaminant cells g⁻¹ basalt) (31). This limited analyses to rocks with small, smectite-dominated cross-cutting veins, which – unlike carbonate-dominated major veins - remained intact during drilling, and could be cracked open and aseptically sampled shipboard after core recovery. All processed samples were stored at -80°C prior to extraction of DNA in the home laboratory.

DNA Extraction. Using sterile spatulas, 2-4 cm² (0.3-0.5 g) of inner vein surfaces were scraped off and DNA extracted following the same protocol as previously for RNA (32) except that the sodium phosphate (NaH₂PO₄) concentration of the extraction buffer was raised to 120 μM, the pH of the extraction buffer and phenol increased to 8.0, and bead-beating reduced to 15 s at a speed of 4.0. Negative controls containing no basalt samples were run in parallel to check for contamination of extraction reagents. Samples and controls were purified with the PowerClean DNA Clean-Up Kit (MOBIO laboratories, Carlsbad, CA).

Primer Selection and PCR Amplification. *mcrA* was PCR-amplified using the *mcrIRD* and ANME-1-*mcrI* primer pairs. These primer pairs target all known and several novel *mcrA* gene clusters when used complementarily, as shown in extensive tests with marine sediment samples (33). *dsrB* was PCR-amplified by nested PCR with published external primers (DSR1F/4R) (14), and a newly designed primer mixture used internally (*dsrB* F1a-h/4RSI1a-f), after tests with published primers had produced negative results (Tables S12 and S13). The PCR protocol consisted of (1) 1×2 min denaturation (98°C), (2) 40× (a) 30s denaturation (95°C), (b) 30s annealing (*mcrIRD*: 55°C; ANME-1-*mcrI*: 63°C; DSR1F/4R: 54°C, *dsrB* F1a-h/4RSI1a-f: 56°C), (c) 1 min extension (72°C), and (3) 1×5 min extension (72°C). In each PCR assay, negative controls for contamination of extraction and PCR reagents were run and found to be negative.

Cloning, sequencing, and phylogenetic analyses. PCR fragments were purified in a 2% low-melting point agarose gel and agarose removed with a S.N.A.P. MiniPrep Kit. Purified DNA was cloned and inserted into electrocompetent *E. coli* using the TOPO TA Kit (both kits by Invitrogen, Carlsbad, USA). All trees were constructed with nucleotides in ARB Neighbour Joining using Jukes-Cantor correction (34).

Nucleotide sequence accession numbers. The GenBank nucleotide accession numbers are GU182109-GU182110, and JX465656-JX465658.

Solid-phase S Analyses. Contents and δ³⁴S-compositions of bulk S pools (AVS, CRS, SO₄-S) were analyzed on rock powders using published protocols (5, 23).

The δ³⁴S of pyrite grains was measured on polished rock thin-sections by SIMS using the mono-collection Cameca IMS 1280 (35), and by LA-MC-ICPMS (Laser

Ablation Multiple Collector Inductively Coupled Plasma Mass Spectrometry) using the NewWave UP213 laser coupled to the Neptune (Thermo) MC-ICP-MS (36). For both techniques, the minimum grain diameter for $\delta^{34}\text{S}$ -determination was 10 μm . In certain samples (e.g. 14R-1, 17R-1, 19R-1), pyrite grains were measured with SIMS and LA-MC-ICPMS and showed agreement within analytical uncertainties. Details of both techniques are outlined in the following paragraphs.

For the SIMS technique, a beam of $^{133}\text{Cs}^+$ ions was used for sputter-ionizing S as negatively charged secondary ions from pyrite grains. A mass resolving power (MRP) of ~ 5000 was used with a primary Cs^+ beam current switched to a spot of ~ 2 mm diameter with a current of ~ 6 pA. Peak calibration and pre-sputtering was made for each spot analysis and the intensity data was then processed by an off-line time-interpolation correction protocol to minimize the effect of variations of the primary beam intensity on measured isotope ratios. Pyrite standards used were: Ruttan (+1.2 ‰ VCDT), MVE04-14-4 (-13.15‰), and Balmat (+15.1‰). For each session, at least two of each were measured repeatedly to ascertain that the instrumental mass fractionation factor (a) was statistically identical for all standards. a varied from session to session and day to day, but was constant during a day. No efforts were made to modify instrument optical parameters on a day-to-day basis to control a .

The LA-MC-ICPMS technique followed a published method (36), in which single-spot analyses were made using a 30 μm diameter beam size with an energy density of $\sim 9\text{--}10$ J cm^{-2} . Standard-sample bracketing was used to correct for the instrumental mass bias of unknown pyrite samples using standard-solutions calibrated against in-house pyrite standards of known composition (GAV-18=10.4‰; ALV-4053=2.5‰).

Solid-phase C Analyses. TOC content was determined by element analyzer (EA). Traces of carbonate C were removed by reaction with dilute (3N) HCl, followed by washing in distilled H_2O (37). $\delta^{13}\text{C}$ -TOC was determined with a Costech EA coupled to a Thermo Scientific Delta V plus isotope ratio MS (IRMS), using IAEA 600 Caffeine ($\delta^{13}\text{C} = -27.77\text{‰}$ VPDB) and IAEA-CH-6 Sucrose (-10.45‰) as calibration standards. Rock powders were degassed at 100°C and stored under vacuum to minimize adsorption of atmospheric CO_2 . Replicate analyses of low-C content samples (<500 ppm) were within ± 70 ppm and $\pm 0.5\text{‰}$ $\delta^{13}\text{C}$. C blanks are less than 6% of reported C contents. $\delta^{13}\text{C}$ -carbonate was analyzed as described previously (10). Since the carbonate content of rocks used for bulk geochemical analyses and smectite-dominated veins used for genetic analyses was too low for $\delta^{13}\text{C}$ -analyses, carbonate-dominated major veins were used.

Basalt enrichments. Methanogen Medium 141 (Deutsche Sammlung von Mikroorganismen und Zellkulturen) was prepared with minor modifications (Table S8). The initial inoculum consisted of fresh basalt shards from rock interiors in which drilling fluid contamination was near or below the detection limit (<0.1 contaminant cells g^{-1} basalt; 1R-1-79, 14R-1-11, 23R-2-21) (31). For transfers, a few incubated basalt pieces were added to fresh medium containing triple-autoclaved basalt pieces and no sulfate. Headspace methane and dissolved species (sulfate, sulfide, DIC) were measured via standard protocols. $\delta^{13}\text{C}$ -methane was determined using a Trace GC coupled via GC combustion III interface to a Delta plus XP plus IRMS (all Thermo Finnigan) following a previously published protocol (38). The absence of color changes due to oxidation of resazurin indicated that media remained fully anoxic throughout incubations.

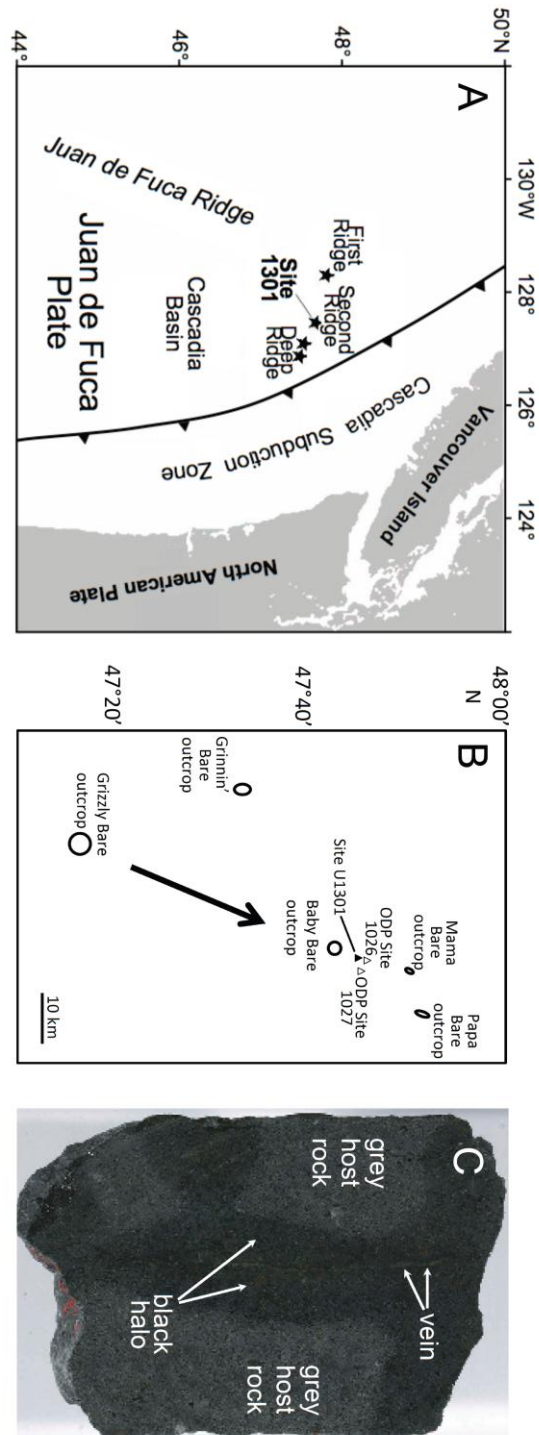


Fig. S1. (A) Map of study area. (B) General direction of subsurface flow from Grizzly Bare outcrop to the Baby Bare Spring area and U1301 (6, 11). (C) Cross section through basalt core from U1301B, showing the alteration halos that surround basalt veins or fractures (adapted from (9)).

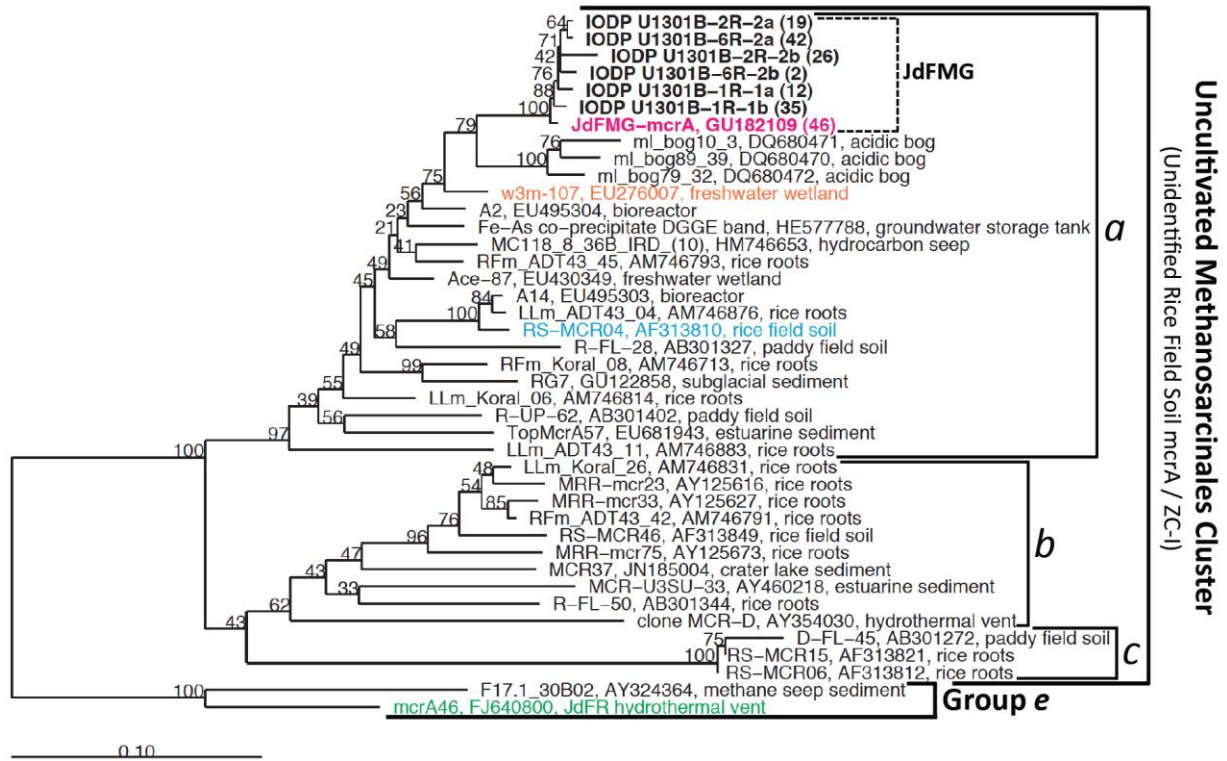


Fig. S2. Phylogenetic tree of the Uncultivated Methanosarcinales Cluster (congruent with the Unidentified Rice Field Soil *mcrA* (15) and Zoige cluster I (ZC-I); 16) based on *mcrA* sequences. The uncultivated Methanosarcinales group *e* is used as an outgroup. All phylotypes detected in this study in bold type face, with the one displayed in Fig. 1a in magenta. Clone numbers sequenced for each phylotype are shown in parentheses. The closely related methanogenic phylotype that was enriched in wetland sediment is in orange (16), the closest relative of an *mcrA* gene detected in Juan de Fuca Ridge seafloor basalt by microarray analysis is in blue (18), and the closest relative from Juan de Fuca Ridge hydrothermal vent chimneys in green (17). Constructed from nucleotides in ARB Neighbour Joining using Jukes-Cantor correction. Bootstrap support (in %, 1,000 replications) is indicated at each branching point.

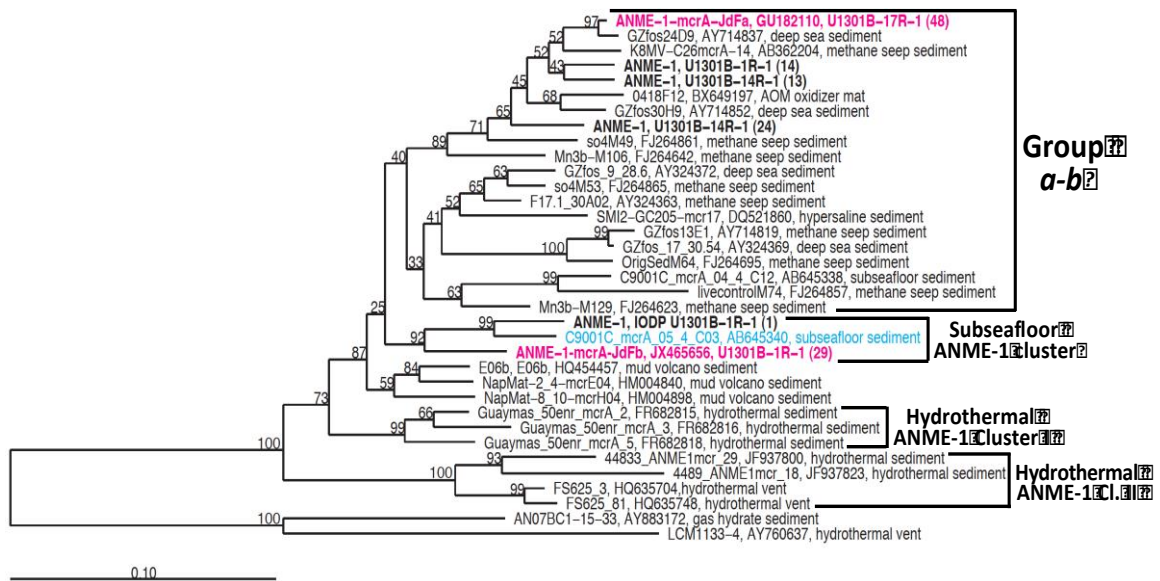


Fig. S3. Phylogenetic tree of ANME-1 based on *mcrA* sequences. All phylotypes from subseafloor basalt of the Juan de Fuca Ridge Flank appear in bold type face, with ones included in Fig. 1A in magenta. Clone numbers sequenced for each phylotype are shown in parentheses. In cyan, the only other deep subseafloor ANME-1 sequence in Genbank, from sediments of the Northwest Pacific off Shimokita Peninsula (Nunoura et al., unpubl.). Highly divergent ANME-1 sequences from the Lost City Hydrothermal Field (LCM1133-4) and gas hydrate sediment (AN07BC1-15-33), which form a distinct cluster of their own, are used as an outgroup. Constructed with nucleotides in ARB Neighbour Joining using Jukes-Cantor correction. Bootstrap support (in %, 1,000 replications) is indicated at each branching point.

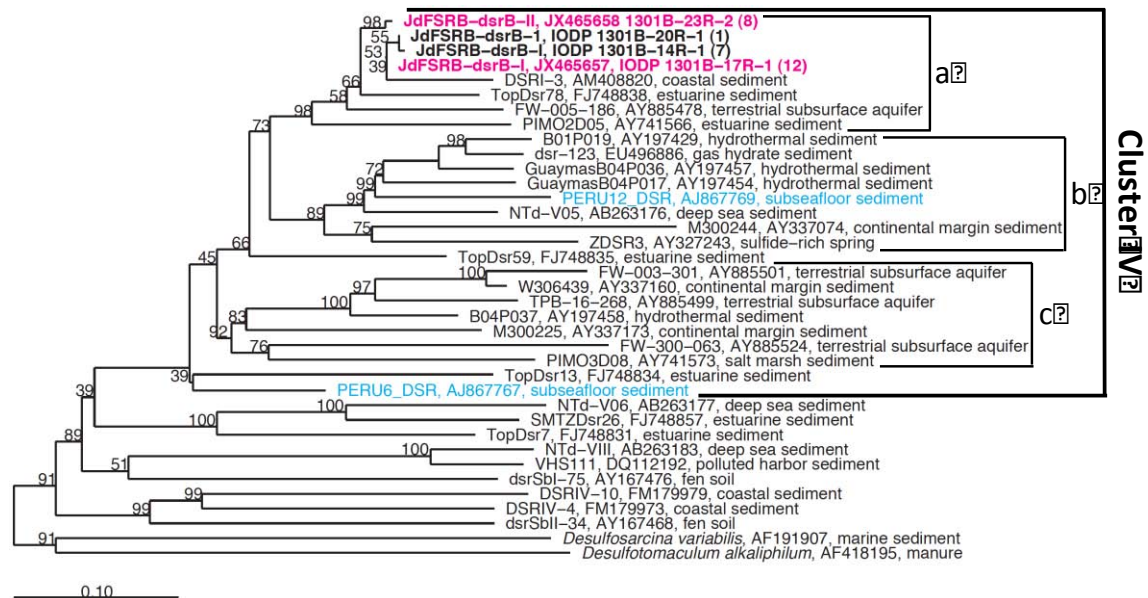


Fig. S4. Phylogenetic tree of Cluster IV and related *dsrB* clusters. Phylotypes from Juan de Fuca Ridge Flank basalt appear in bold type face, with ones shown in Fig. 1B in magenta. Clone numbers sequenced for each phylotype are shown in parentheses. Sequences detected in subsurface sediment of the Peru Margin are shown in blue (S20). Cluster IV falls into at least 3 distinct subclusters (*a-c*) that each have high bootstrap support (>85%). All JdFSRG fall into subcluster *a*. Constructed with nucleotides in ARB Neighbour Joining using Jukes-Cantor correction. Sequences of Desulfobacteraceae (*Desulfosarcina variabilis*) and Firmicutes (*Desulfotomaculum alkaliphilum*) used as outgroups. Bootstrap support (in %, 1,000 replicates) shown at each branching point.

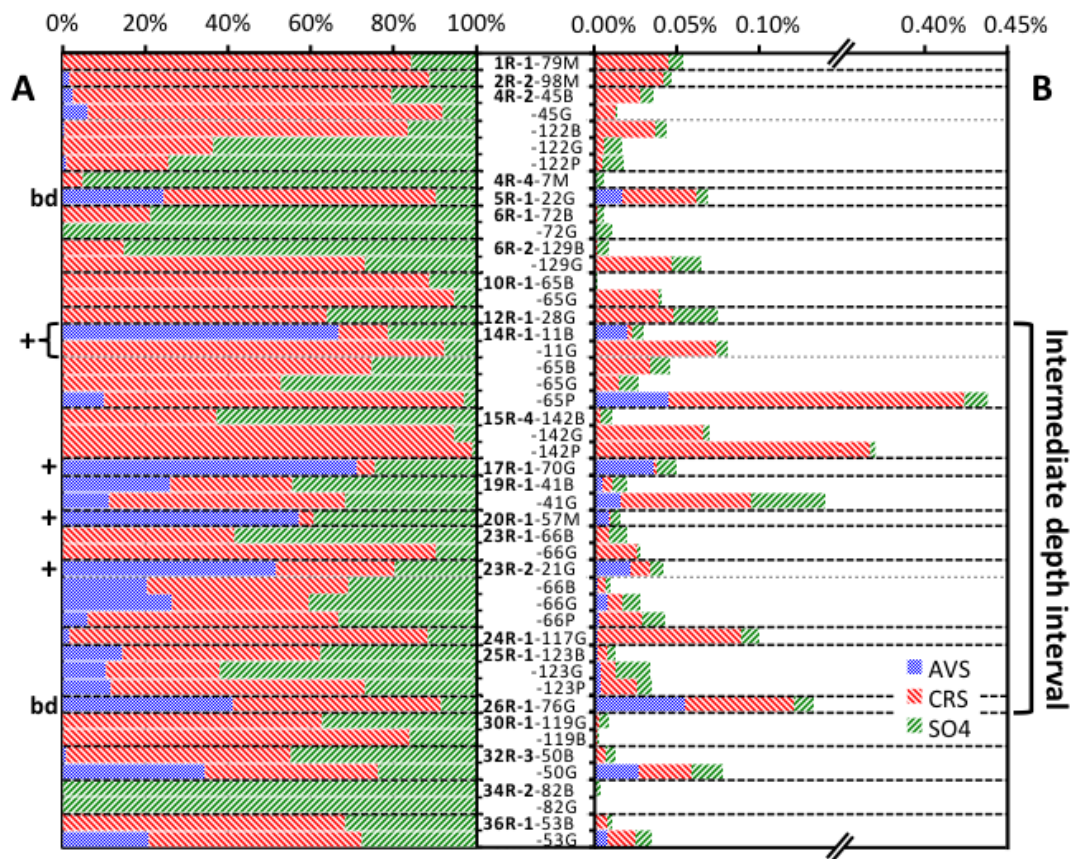


Figure S5. (A) Relative weight contributions of AVS, CRS, and SO₄-S to total S; (B) Cumulative weight contributions of AVS, CRS, and SO₄-S to total basalt sample. Sample IDs are shown in the middle. Rock samples in which DNA extracts were tested for *dsrB* presence are indicated on the far left. All data is listed in Table S2. B = black alteration halo; G = grey host rock; P = pyrite front a narrow zone (typically <0.1mm) of concentrated disseminated pyrite along the boundary between an alteration halo and the adjacent host rock, located at interface of black alteration halo and grey host rock; M = mixed lithology.

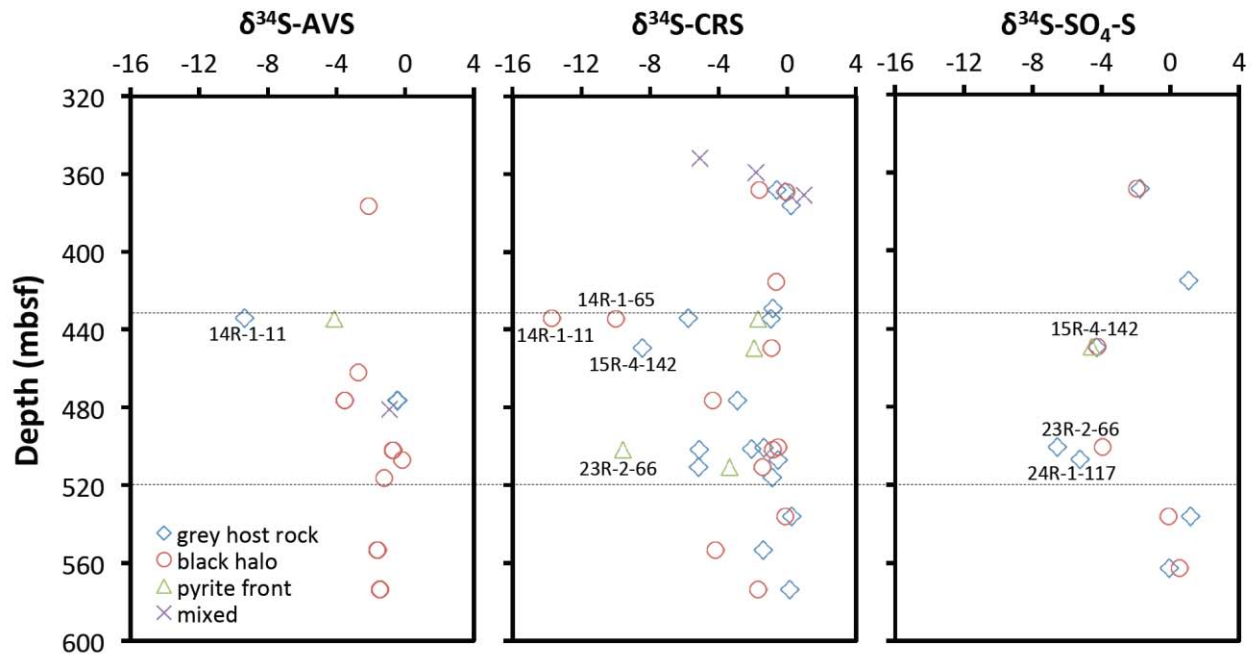


Fig. S6. Depth-related trends in $\delta^{34}\text{S}$ of CRS, AVS, and $\text{SO}_4\text{-S}$ at IODP Site U1301. The more reduced intermediate depth interval falls between the dashed lines. All $\delta^{34}\text{S}$ -values are expressed in ‰ vs. VCDT.

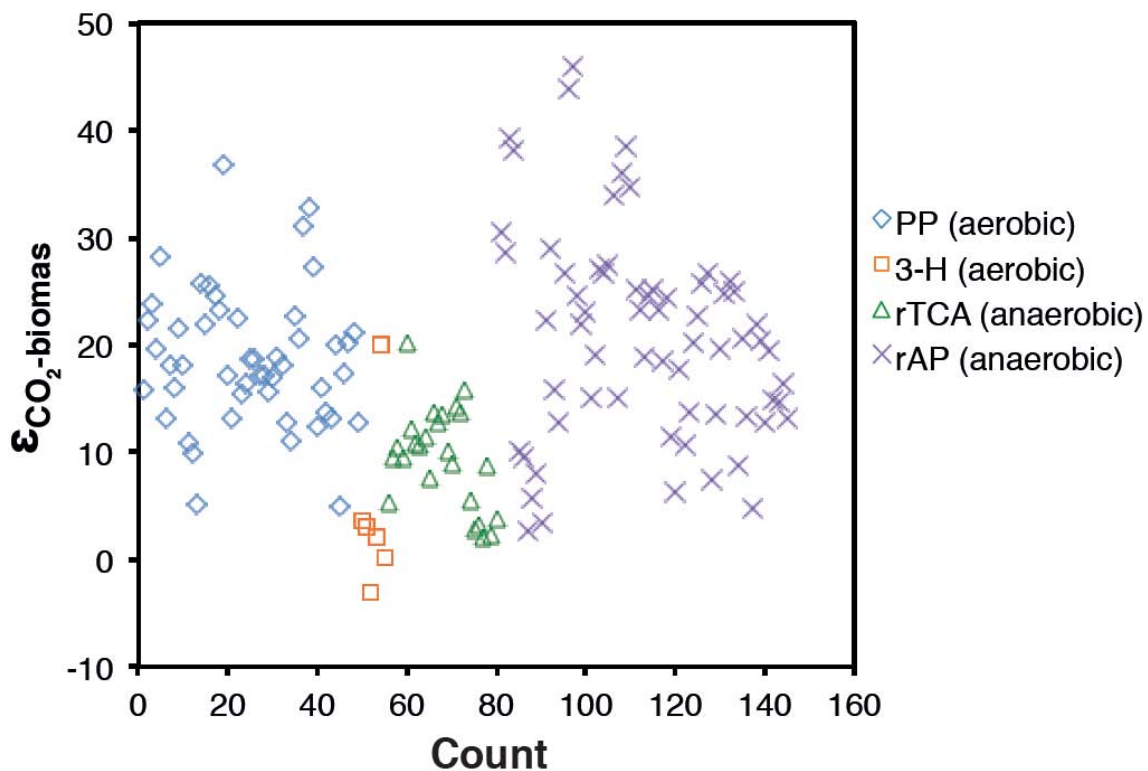


Fig. S7. Compiled data from Table S6 on $\delta^{13}\text{C}$ -fractionations associated with aerobic and anaerobic C-fixation pathways. Abbreviations: PP = pentose phosphate (Calvin-Benson-Bassham) cycle, 3-H = 3-hydroxypropionate cycle, rTCA = reverse tricarboxylic acid cycle, rAP = reductive acetyl CoA pathway. Note that the PP pathway also occurs in some anoxygenic phototrophs (*Chromatium*, *Thiocapsa*, *Rhodospirillum*; Table S6).

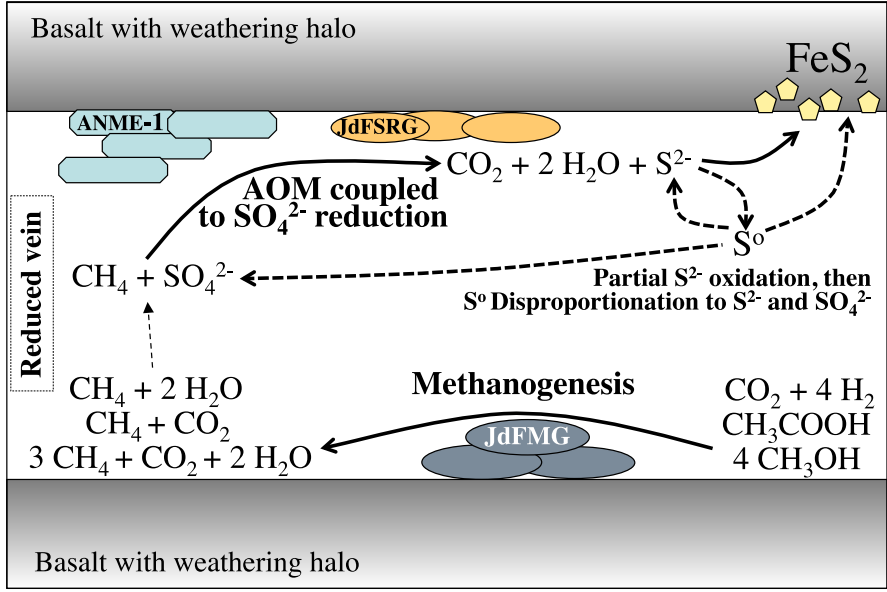


Fig. S8. Concept sketch of microbial methane and S-cycling in reduced veins of Juan de Fuca subsurface basalt (e.g. core 17R-1-70). Potential methanogenic substrates include H₂/CO₂, acetate, and methylated organic substrates. Methanogens, methanotrophs and sulfate reducers may coexist (as shown) or inhabit separate chemical microenvironments.

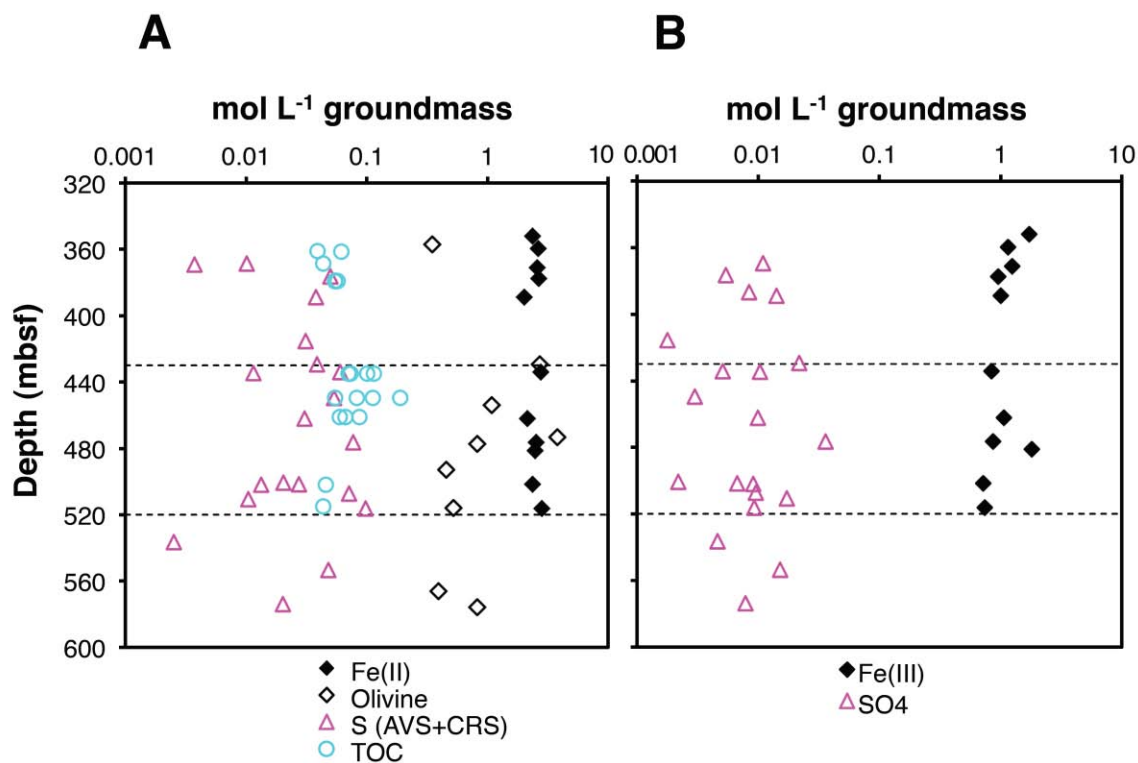


Fig. S9. (A) Molar contents of the potential electron donors Fe(II), reduced S (includes both AVS- and CRS-S), and TOC per liter of basalt groundmass in borehole U1301B. Values for Fe(II) in olivine ((Mg, Fe)₂SiO₄) are also shown. (B) Molar contents of the potential electron acceptors Fe(III) and SO₄ per liter of groundmass at U1301B. The more reduced intermediate depth interval falls between the dashed lines. Except for olivine, which was obtained from Fisher et al. (2005; 9), all data from this study. See Table S10 for a listing of potential energy-yielding reactions in borehole U1301B.

Table S1. Sample identity, depth, lithology, total S and TOC content in host rock and halos (n=sample size), Fe(II) fraction of total Fe (FeT), $\delta^{34}\text{S}$ -pyrite, $\delta^{34}\text{S}$ -CRS and -AVS of host rock¹ and halos¹ (halos in parentheses), $\delta^{13}\text{C}$ -TOC, *mcrA* and *dsrB* clone library composition with number of clones obtained for each phylotype in parentheses. [wt% = % of sample weight, bd = below detection; nd = not determined; $\delta^{13}\text{C}$ -values in ‰ vs. Vienna Pee Dee Belemnite (VPDB), $\delta^{34}\text{S}$ in ‰ vs. Vienna-Canyon Diablo Troilite (VCDT).]

¹ host rock = main basalt type; exhibits a pervasive dark gray background alteration manifest by secondary saponite; halo = distinctly colored band of rock (typically 1-15mm wide) flanking a vein; color imparted by differing secondary minerals (black halos contain celadonite, brown halos contain iron oxy-hydroxide).

Sample ID ²	Depth (mbsf)	Lithology ³	Total S (wt%) ⁴	TOC (wt%)	Fe ³⁺ /FeT ⁵	$\delta^{34}\text{S}$ (‰)			$\delta^{13}\text{C}$ -TOC (‰)	<i>mcrA</i> cluster (# of clones)	<i>dsrB</i> cluster (# of clones)
						pyrite (‰)	CRS (‰) ⁶	AVS (‰) ⁶			
1R-1-79	352.0	20% breccia and pillow basalt (30% black halo) with small disseminated sulfide grains	0.04	nd	0.42	bd	-5.1	nd	nd	JdFMG (47), ANME-1 (44)	nd
2R-2-98	359.6	pillow basalt, brown/black halos (80%)	0.06	0.017-0.027 (n=3) ⁶	0.30	bd	-1.8	nd	-21.6 to -26.6 (n=3) ⁷	JdFMG (45)	nd
4R-4-7	371.2	pillow basalt, brown halo (Fe oxides)	0.05	0.019 (halo 0.025) ⁶	0.32	bd	1	nd	-34.6 (halo -34.0) ⁷	bd	nd
5R-1-22	377.5	pillow basalt, close to pillow rim	0.09	0.024-0.025 (n=4) ⁶	0.26	bd	0.2	-2.1	-32.0 to -32.8 (n=4) ⁷	bd	bd
6R-2-129	388.8	pillow basalt with black halo	0.07 (halo 0.03)	nd	0.33 (halo 0.47)	bd	-2.7	nd	nd	JdFMG (44)	nd
14R-1-11	434.1	massive basalt with black halo (pyrite disseminated in groundmass)	0.12 (halo 0.10)	0.031-0.050 (n=4)	0.23 (halo 0.38)	-4 to -47	-5.7 (-13.7)	(-9.3)	-21.9 to -26.5 (n=4)	ANME-1 (37)	Group IV (7)
17R-1-70	462.1	pillow basalt with black halo, pyrite in groundmass and along veins	0.10 (halo 0.04)	0.026-0.038 (n=3)	0.33 (halo 0.41)	-35 to -72	nd	-2.7	-26.0 to -27.6 (n=3)	JdFMG (46), ANME-1 (48)	Group IV (12)
20R-1-57	481.2	pillow basalt with oxidized groundmass (no pyrite)	0.03	nd	0.42	bd	nd	-0.9	nd	bd	Group IV (1)
23R-2-21	501.6	pillow basalt with black halo, only a single pyrite crystal found; brown halo	0.05 (halo 0.07)	0.020	0.23 (halo 0.24)	-2 to -3	-2.1	0.0 (0.0)	-33.5	bd	Group IV (8)
26R-1-76	516.3	pillow basalt with black halo, no pyrite found	0.13 (halo 0.08)	0.019	0.21 (halo 0.28)	bd	-0.9	-1.22	-33.9	bd	bd

² Sample designation as follows: 1R-1-79 = core 1, sampled by Rotary Core Barrel (R), section 1, 79 cm from section top

³ from (9)

⁴ total S determined by elemental analyzer

⁵ Fe²⁺ determined by titration, total Fe (FeT) by Inductively Coupled Plasma Atomic Emission Spectroscopy (ICP-AES), Fe³⁺ calculated from difference.

⁶ only samples with detectable CRS or AVS were analyzed.

⁷ values from within the same core, but not from the same rock used for genetic analyses (also see Table S3).

Table S2. Solid-phase S weight % (wt %) of basalt (wt %), relative contributions of different S pools to total S (%), and $\delta^{34}\text{S}$ of these same S pools. Bold font indicates samples also used for DNA extractions [bd = below detection; - = not determined; $\delta^{34}\text{S}$ in ‰ vs. VCDT.]

	Depth mbsf	S pools (wt %)				% contributions			$\delta^{34}\text{S}$		
		AVS	CRS	SO ₄ -S	Total	AVS	CRS	SO ₄ -S	AVS	CRS	SO ₄ -S
1R-1-79M	352.0	0.00	0.05	0.01	0.05	0	84	16	bd	-5.1	-
2R-2-98M	359.6	0.00	0.04	0.01	0.05	2	87	12	bd	-1.8	-
4R2-45B	368.5	0.00	0.03	0.01	0.04	2	77	21	bd	-1.6	-1.9
4R2-45G	368.5	0.00	0.01	0.00	0.01	6	86	8	bd	-0.6	-1.7
4R-2-122B	369.3	0.00	0.04	0.01	0.04	1	83	17	bd	-0.1	-
4R-2-122G	369.3	0.00	0.01	0.01	0.02	0	37	63	bd	-0.1	-
4R-2-122P	369.3	0.00	0.00	0.01	0.02	1	25	74	bd	bd	-
4R-4-7M	371.2	0.00	0.00	0.01	0.01	0	5	95	bd	1.0	-
5R-1-22G	376.5	0.02	0.05	0.01	0.07	25	66	10	-2.1	0.2	-
6R-1-72B	386.7	0.00	0.00	0.00	0.01	0	21	79	bd	bd	-
6R-1-72G	386.7	0.00	0.00	0.01	0.01	0	0	100	bd	bd	-
6R-2-129B	388.8	0.00	0.00	0.01	0.01	0	15	85	bd	bd	-
6R-2-129G	388.8	0.00	0.05	0.02	0.06	0	73	27	bd	-2.7	-
10R1-65B	415.5	0.00	0.00	0.00	0.00	0	89	11	bd	-0.7	bd
10R1-65G	415.5	0.00	0.04	0.00	0.04	0	95	5	bd	bd	1.1
12R-1-28G	429.2	0.00	0.05	0.03	0.07	0	64	36	bd	-0.8	-
14R-1-11B	434.1	0.02	0.00	0.01	0.03	67	12	21	-9.3	-13.7	-
14R-1-11G	434.1	0.00	0.07	0.01	0.08	0	92	8	bd	-5.7	-
14R-1-65B	434.7	0.00	0.03	0.01	0.05	0	75	25	bd	-9.9	-
14R-1-65G	434.7	0.00	0.01	0.01	0.03	0	53	47	bd	-0.9	-
14R-1-65P	434.7	0.04	0.38	0.01	0.44	10	87	3	-4.1	-1.7	-
15R4-142B	449.5	0.00	0.00	0.01	0.01	0	37	63	bd	-0.9	-4.2
15R4-142G	449.5	0.00	0.07	0.00	0.07	0	95	5	bd	-8.4	-4.3
15R4-142P	449.5	0.00	0.37	0.00	0.37	0	99	1	bd	-1.9	-4.6
17R-1-70G	462.1	0.04	0.00	0.01	0.05	71	5	24	-2.7	bd	-
19R-1-41B	476.5	0.01	0.01	0.01	0.02	26	30	44	-0.5	-4.4	-
19R-1-41G	476.5	0.02	0.08	0.04	0.14	11	57	32	-3.5	-2.9	-
20R-1-57M	481.2	0.01	0.00	0.01	0.02	57	3	39	-0.9	bd	-
23R1-66B	500.6	0.00	0.01	0.01	0.02	0	42	58	bd	-0.5	-3.9
23R1-66G	500.6	0.00	0.03	0.00	0.03	0	90	10	bd	-1.3	-6.5
23R-2-21G	501.6	0.02	0.01	0.01	0.04	52	29	20	bd	-2.1	-
23R-2-66B	502.0	0.00	0.00	0.00	0.01	21	49	31	bd	-0.8	-
23R-2-66G	502.0	0.01	0.01	0.01	0.03	26	33	40	-0.7	-5.1	-
23R-2-66P	502.0	0.00	0.03	0.01	0.04	6	61	33	bd	-9.6	-
24R1-117G	507.1	0.00	0.09	0.01	0.10	2	86	12	-0.2	-0.5	-5.2
25R-1-123B	510.7	0.00	0.01	0.00	0.01	14	48	38	bd	-1.5	-
25R-1-123G	510.7	0.00	0.01	0.02	0.03	10	27	62	bd	-5.2	-
25R-1-123P	510.7	0.00	0.02	0.01	0.03	12	61	27	bd	-3.4	-

26R-1-76G	516.3	0.05	0.07	0.01	0.13	41	50	9	-1.2	-0.9	-
30R1-119G	536.4	0.00	0.00	0.01	0.01	0	35	21	bd	0.3	1.2
30R1-119B	536.4	0.00	0.00	0.00	0.00	0	42	8	bd	-0.1	-0.1
32R-3-50B	553.4	0.00	0.01	0.01	0.01	1	54	45	bd	-4.2	-
32R-3-50G	553.4	0.03	0.03	0.02	0.08	34	42	24	-1.6	-1.4	-
34R2-82B	562.9	0.00	0.00	0.00	0.00	0	0	21	bd	bd	0.6
34R2-82G	562.9	0.00	0.00	0.00	0.00	0	0	8	bd	bd	0.0
36R-1-53B	573.7	0.00	0.01	0.00	0.01	0	68	32	bd	-1.7	-
36R-1-53G	573.7	0.01	0.02	0.01	0.03	21	51	28	-1.5	0.1	-

Table S3. Listing of individual $\delta^{34}\text{S}$ measurements by SIMS and laser ablation. In cases where only one measurement was made per granule, the $\delta^{34}\text{S}$ -pyrite and mean $\delta^{34}\text{S}$ per pyrite granule are identical. All $\delta^{34}\text{S}$ are in ‰ versus VCDT. Samples in bold were also used for DNA extractions.

Analy- sis Type	Core ID	Depth (mbsf)	Granule ID	Granule Subsample ID	$\delta^{34}\text{S}$	Standard deviation	Mean $\delta^{34}\text{S}$
<i>laser</i>	13R-1	430.8	13	a	-46.4	0.2	-46.4
<i>laser</i>	13R-1	430.8	1	a	-40.5	0.3	-45.3
<i>laser</i>	13R-1	430.8	1	b	-51.3	0.2	
<i>laser</i>	13R-1	430.8	1	c	-45.3	0.2	
<i>laser</i>	13R-1	430.8	1	d	-32.2	0.2	
<i>laser</i>	13R-1	430.8	1	e	-50.6	0.3	
<i>laser</i>	13R-1	430.8	1	f	-51.0	0.3	
<i>laser</i>	13R-1	430.8	1	g	-46.0	0.3	
<i>laser</i>	13R-1	430.8	1	h	-45.3	0.2	
<i>laser</i>	13R-1	430.8	2	a	-2.4	0.2	-2.4
<i>laser</i>	13R-1	430.8	3	a	-3.9	0.2	-3.9
<i>laser</i>	13R-1	430.8	4	a	-3.4	0.2	-3.4
<i>laser</i>	13R-1	430.8	5	a	-3.4	0.2	-3.3
<i>laser</i>	13R-1	430.8	5	b	-3.4	0.3	
<i>laser</i>	13R-1	430.8	5	c	-3.1	0.2	
<i>laser</i>	13R-1	430.8	6	a	-3.4	0.2	-3.3
<i>laser</i>	13R-1	430.8	6	b	-3.2	0.2	
<i>laser</i>	13R-1	430.8	7	a	-3.5	0.2	-3.8
<i>laser</i>	13R-1	430.8	7	b	-4.2	0.2	
<i>laser</i>	13R-1	430.8	8	a	-3.9	0.2	-3.9
<i>laser</i>	13R-1	430.8	9	a	-3.7	0.2	-3.7
<i>laser</i>	13R-1	430.8	10	a	-4.6	0.2	-4.6
<i>laser</i>	13R-1	430.8	11	a	-5.6	0.2	-5.6
<i>laser</i>	13R-1	430.8	12	a	-5.9	0.2	-5.4
<i>laser</i>	13R-1	430.8	12	b	-5.2	0.2	
<i>laser</i>	13R-1	430.8	12	c	-5.1	0.2	
<i>laser</i>	14R-1-11	434.7	1	a	-23.5	0.3	-25.8
<i>laser</i>	14R-1-11	434.7	1	b	-28.1	0.2	
<i>laser</i>	14R-1-11	434.7	2	a	-22.9	0.2	-21.7
<i>laser</i>	14R-1-11	434.7	2	b	-20.4	0.2	
<i>laser</i>	14R-1-11	434.7	3	a	0.4	0.2	0.3
<i>laser</i>	14R-1-11	434.7	3	b	0.8	0.2	
<i>laser</i>	14R-1-11	434.7	3	c	-0.2	0.2	
<i>laser</i>	14R-1-11	434.7	4	a	0.3	0.2	0.5
<i>laser</i>	14R-1-11	434.7	4	b	0.7	0.2	
<i>laser</i>	14R-1-11	434.7	5	a	-0.2	0.2	-0.2
<i>laser</i>	14R-1-11	434.7	6	a	-29.9	0.4	-32.2

<i>laser</i>	14R-1-11	434.7	6	b	-34.4	0.3	
<i>laser</i>	14R-1-11	434.7	7	a	-33.8	0.2	-35.2
<i>laser</i>	14R-1-11	434.7	7	b	-36.5	0.3	
<i>laser</i>	14R-1-11	434.7	8	a	0.4	0.2	0.7
<i>laser</i>	14R-1-11	434.7	8	b	1.1	0.2	
<i>laser</i>	14R-1-11	434.7	9	a	-46.6	0.2	-29.8
<i>laser</i>	14R-1-11	434.7	9	b	-13.0	0.2	
<i>laser</i>	14R-1-11	434.7	10	a	-7.7	0.2	-7.7
<i>laser</i>	14R-1-11	434.7	11	a	-4.9	0.2	-4.9
<i>laser</i>	14R-1-11	434.7	12	a	-8.7	0.3	-8.7
<i>laser</i>	14R-1-11	434.7	13	a	-9.0	0.3	-9.0
<i>sims</i>	14R-1-11	434.7	14	a	-10.4	0.5	-10.4
<i>sims</i>	14R-1-11	434.7	15	a	-3.3	0.7	-3.3
<i>sims</i>	14R-1-11	434.7	16	a	-19.4	0.6	-19.4
<i>laser</i>	15R-2	445.9	1	a	-7.4	0.2	-7.2
<i>laser</i>	15R-2	445.9	1	b	-10.0	0.2	
<i>laser</i>	15R-2	445.9	1	c	-10.0	0.2	
<i>laser</i>	15R-2	445.9	1	d	-1.2	0.2	
<i>laser</i>	15R-2	445.9	2	a	-0.9	0.2	-0.9
<i>laser</i>	15R-2	445.9	3	a	-1.1	0.2	-1.1
<i>laser</i>	15R-2	445.9	4	a	-1.7	0.2	-1.7
<i>laser</i>	15R-2	445.9	5	a	-8.2	0.2	-8.2
<i>laser</i>	15R-2	445.9	6	a	-19.3	0.2	-19.3
<i>laser</i>	15R-2	445.9	7	a	-3.8	0.2	-8.6
<i>laser</i>	15R-2	445.9	7	b	-8.2	0.2	
<i>laser</i>	15R-2	445.9	7	c	-6.0	0.4	
<i>laser</i>	15R-2	445.9	7	d	-16.3	0.2	
<i>laser</i>	15R-2	445.9	8	a	-2.4	0.2	-2.4
<i>laser</i>	15R-2	445.9	9	a	-3.2	0.2	-3.2
<i>laser</i>	15R-2	445.9	10	a	-4.2	0.2	-4.2
<i>laser</i>	15R-2	445.9	11	a	-13.8	0.2	-13.8
<i>laser</i>	15R-2	445.9	12	a	-1.9	0.2	-1.9
<i>laser</i>	15R-2	445.9	13	a	-1.6	0.2	-1.6
<i>laser</i>	15R-2	445.9	14	a	-9.7	0.2	-9.7
<i>sims</i>	15R-2	445.9	1	a	-0.3	0.3	-0.3
<i>sims</i>	15R-2	445.9	2	a	-2.9	0.3	-2.9
<i>sims</i>	15R-2	445.9	3	a	-25.9	0.3	-25.9
<i>sims</i>	15R-2	445.9	4	a	-22.6	0.3	-22.6
<i>sims</i>	15R-2	445.9	5	a	-1.6	0.4	-1.6
<i>sims</i>	15R-2	445.9	6	a	-11.7	0.5	-11.7
<i>sims</i>	15R-2	445.9	7	a	-17.5	0.4	-17.5
<i>sims</i>	15R-2	445.9	8	a	-7.9	0.5	-7.9
<i>sims</i>	15R-2	445.9	9	a	-2.7	0.5	-2.7
<i>sims</i>	15R-2	445.9	10	a	-1.9	0.5	-1.9
<i>sims</i>	15R-2	445.9	11	a	-5.7	0.5	-5.7
<i>laser</i>	15R-4	449.5	1	a	-1.8	0.2	-1.8

<i>laser</i>	15R-4	449.5	1	b	-1.7	0.2	
<i>laser</i>	15R-4	449.5	2	a	-1.3	0.2	-1.3
<i>laser</i>	15R-4	449.5	3	a	-1.4	0.2	-1.5
<i>laser</i>	15R-4	449.5	3	b	-1.6	0.2	
<i>laser</i>	17R-1-70	461.8	1	a	-65.1	0.2	-65.1
<i>laser</i>	17R-1-70	461.8	2	a	-69.0	0.2	-69.4
<i>laser</i>	17R-1-70	461.8	2	b	-70.1	0.2	
<i>laser</i>	17R-1-70	461.8	2	c	-69.4	0.2	
<i>laser</i>	17R-1-70	461.8	2	d	-69.0	0.2	
<i>laser</i>	17R-1-70	461.8	4	a	-63.4	0.3	-63.4
<i>laser</i>	17R-1-70	461.8	5	a	-68.5	0.2	-68.5
<i>laser</i>	17R-1-70	461.8	6	a	-35.2	0.2	-35.2
<i>sims</i>	17R-1-70	461.8	7	a	-70.4	0.4	-70.4
<i>sims</i>	17R-1-70	461.8	8	a	-72.4	0.4	-72.4
<i>sims</i>	17R-1-70	461.8	9	a	-71.2	0.5	-71.2
<i>sims</i>	17R-1-70	461.8	10	a	-71.5	0.3	-71.5
<i>sims</i>	17R-1-70	461.8	11	a	-58.6	0.4	-58.6
<i>laser</i>	18R-2	473.1	1	a	-31.0	0.2	-30.1
<i>laser</i>	18R-2	473.1	1	b	-29.1	0.3	
<i>laser</i>	18R-2	473.1	2	a	-14.0	0.3	-9.9
<i>laser</i>	18R-2	473.1	2	b	-5.9	0.3	
<i>laser</i>	18R-2	473.1	3	a	-0.2	0.2	-13.1
<i>laser</i>	18R-2	473.1	3	b	-25.5	0.3	
<i>laser</i>	18R-2	473.1	3	c	-0.9	0.2	
<i>laser</i>	18R-2	473.1	3	d	-18.0	0.7	
<i>laser</i>	18R-2	473.1	3	e	-20.9	0.3	
<i>laser</i>	18R-2	473.1	4	a	-1.4	0.2	-4.9
<i>laser</i>	18R-2	473.1	4	b	-8.4	0.2	
<i>laser</i>	18R-2	473.1	5	a	-7.7	0.4	-3.5
<i>laser</i>	18R-2	473.1	5	b	0.8	0.2	
<i>laser</i>	18R-2	473.1	6	a	-15.9	0.2	-13.8
<i>laser</i>	18R-2	473.1	6	b	-11.8	0.2	
<i>laser</i>	18R-2	473.1	7	a	1.2	0.3	0.7
<i>laser</i>	18R-2	473.1	7	b	0.2	0.2	
<i>laser</i>	19R-1	476.5	2	a	-47.0	0.2	-47.8
<i>laser</i>	19R-1	476.5	2	b	-51.2	0.2	
<i>laser</i>	19R-1	476.5	2	c	-45.2	0.2	
<i>laser</i>	19R-1	476.5	3	a	-61.7	0.2	-62.5
<i>laser</i>	19R-1	476.5	3	b	-63.3	0.2	
<i>laser</i>	19R-1	476.5	4	a	-62.1	0.4	-62.1
<i>laser</i>	19R-1	476.5	5	a	-64.3	0.2	-64.3
<i>laser</i>	19R-1	476.5	6	a	-47.2	0.2	-47.2
<i>sims</i>	19R-1	476.5	7	a	-62.8	0.3	-62.8
<i>sims</i>	19R-1	476.5	8	a	-65.7	0.5	-65.7
<i>sims</i>	19R-1	476.5	9	a	-66.8	0.4	-66.8
<i>sims</i>	19R-1	476.5	10	a	-66.7	0.6	-66.7

<i>sims</i>	19R-1	476.5	11	a	-47.0	0.9	-47.0
<i>sims</i>	19R-1	476.5	12	a	-61.9	0.5	-61.9
<i>sims</i>	19R-1	476.5	13	a	-42.5	0.4	-42.5
<i>laser</i>	23R-2-21	501.4	1	a	-2.7	0.2	-2.2
<i>laser</i>	23R-2-21	501.4	1	b	-1.6	0.2	

Table S4. Summary of $\delta^{13}\text{C}$ -TOC and TOC content data. *n* indicates the number of subsamples analyzed. Values of individual subsamples are indicated in italic, where more than 1 subsample was analyzed. $\delta^{13}\text{C}$ -values are expressed in ‰ vs. VPDB, TOC content in wt. % of total basalt. [* = same sample also used for genetic analyses; - = not determined; G = grey host rock, B = black halo.]

Core ID	<i>n</i>	Depth (mbsf)	$\delta^{13}\text{C}$ ($\pm\text{SD}$)	Wt. %
2R-3-93	1	361.0	-21.6	-
2R-3-115	1	361.3	-26.6	0.017
2R-3-134	1	361.4	-23.7	0.027
4R-2-45B	1	368.6	-34.0	0.025
4R-2-45G	1	368.6	-34.6	0.019
5R-2-126 (mean)	4	379.1	-32.6 \pm 0.4	0.024 (\pm 0.001)
<i>5R-2-126a</i>			-32.8	<i>0.025</i>
<i>5R-2-126b</i>			-32.8	<i>0.024</i>
<i>5R-2-126c</i>			-32.0	<i>0.024</i>
<i>5R-2-126d</i>			-32.8	<i>0.024</i>
14R-1-11 (mean)*	4	434.1	-23.8 \pm 2.0	0.039 (\pm 0.009)
<i>14R-1-11a</i>			-26.5	<i>0.031</i>
<i>14R-1-11b</i>			-24.0	<i>0.032</i>
<i>14R-1-11c</i>			-21.9	<i>0.050</i>
<i>14R-1-11d</i>			-22.6	<i>0.044</i>
15R-4-142 (mean)	4	443.6	-27.9 \pm 0.4	0.048 (\pm 0.025)
<i>15R-4-142a</i>			-28.4	<i>0.024</i>
<i>15R-4-142b</i>			-27.9	<i>0.049</i>
<i>15R-4-142c</i>			-27.9	<i>0.036</i>
<i>15R-4-142d</i>			-27.5	<i>0.083</i>
17R-1-70 (mean)*	3	462.1	-26.9 \pm 0.8	0.031 (\pm 0.006)
<i>17R-1-70a</i>			-27.6	<i>0.026</i>
<i>17R-1-70b</i>			-27.2	<i>0.029</i>
<i>17R-1-70c</i>			-26.0	<i>0.038</i>
23R-2-21*	1	499.9	-33.5	0.020
26R-1-76*	1	515.5	-33.9	0.019

Table S5. Overview of $\delta^{13}\text{C}$ -carbonate values. All measurements expressed in ‰ vs. VPDB.

Sample	Depth (mbsf)	$\delta^{13}\text{C}$
5R-3-47	379.8	0.06
12R-1-28	429.2	-1.78
18R-2-27	472.6	-5.07
18R-2-34	472.6	-4.68
18R-2-55	472.9	-4.06
18R-3-16	473.7	-3.87
18R-3-49	474.1	-2.80
18R-3-88	474.4	-3.36
18R-3-106	474.6	-3.49
18R-3-118	474.7	-1.74
18R-4-0	474.9	-2.97
18R-4-9	475.0	-3.94
35R-2-49	565.6	-1.78

Table S6. Compilation of $\delta^{13}\text{C}$ -isotopic fractionations from carbon dioxide (CO_2) to cell biomass across known C-fixation pathways. Data compiled from seven different studies (26, 39-44) and references within. All data from pure cultures except where marked with an asterisk - asterisks indicate measurements on natural samples. Pathway means and standard deviations were determined on strain averages, where more than one published value was available. PP = pentose phosphate cycle (Calvin Benson Bassham Cycle), 3-H = 3-hydroxypropionate cycle, rTCA = reverse tricarboxylic acid cycle, rAP = reductive acetyl CoA pathway, ϵ_{CO_2} to cells = C-isotopic fractionation from CO_2 to cell biomass, N/A = not applicable.

Count	Path-way	Organism	T _{growth} (°C)	ε _{CO2-cell}			Ref.
				strain (‰)	strain mean (‰)	strain SD (‰)	
1	PP	Agmenellum quadrupicatum	39	15.9	20.4	3.5	26
2	PP	" "	39	22.2			26
3	PP	" "	39	23.9			26
4	PP	" "	39	19.6			26
5	PP	Alkaligenes eutrophus	28	28.2	28.2		26
6	PP	Anacystis nidulans	39	13.1	17.3	3.1	26
7	PP	" "	39	18			26
8	PP	" "	33	16			26
9	PP	" "	33	21.5			26
10	PP	" "	33	18			26
11	PP	Rhodopseudomonas capsulata		10.8	10.4		26
12	PP	" "	30	9.9			26
13	PP	Thiobacillus novellus*	30	5.1	5.1		39
14	PP	Thiobacillus neapolitanus*		25.8	25.8		26
15	PP	Thiocapsa roseopersicina*	28	22	22.0		26
16	PP	Thiomicrospira sp. L-12*		25.5	25.5		26
17	PP	Thiomicrospira crunogena*		24.5	24.5		26
18	PP	Thiomicrospira crunogena*		23.3	23.3		26
19	PP	Chlamydomonas reinhardtii*	20	36.8	36.8		26
20	PP	Microcoleus chthonoplastes	39	17.1	17.1		26
21	PP	Schizothrix calcicola	39	13.2	13.2		26
22	PP	Synechococcus sp.	57	22.5	17.8	2.0	26
23	PP	" "		15.5			26
24	PP	" "		16.4			26
25	PP	" "		18.6			26
26	PP	" "		18.6			26
27	PP	" "		17.2			26
28	PP	" "		17.1			26
29	PP	" "		15.6			26
30	PP	" "		16.9			26
31	PP	" "		18.9			26
32	PP	" "		18.1			26
33	PP	Synechococcus lividus	47	12.8	12.0		26
34	PP	" "	70	11.1			26
35	PP	Chlorella sorokiniana	39	22.6	22.6		26
36	PP	Chromatium tepidum	50	20.5	20.5		26

37	PP	Chromatium strain D*	20	31	31.9		26
38	PP	" " *	20	32.7			26
39	PP	Chromatium vinosum*	20	27.3	27.3		26
40	PP	Coccochloris elebens	39	12.3	14.2		26
41	PP	" "	39	16			26
42	PP	Nitrosomonas europaea*		13.8	15.7	3.8	26
43	PP	" " *		13.2			26
44	PP	" "		20			40
45	PP	Oscillatoria williamsii	39	5	11.2		26
46	PP	" "	39	17.3			26
47	PP	Oscillochloris trichoides*	28	20.1	20.1		26
48	PP	Rhodospirillum rubrum	20	21.1	16.9		26
49	PP	" "	20	12.7			26
50	3-H	Acidianus brierleyi	65	3.6	3.6		39
51	3-H	Metallosphaera sedula	65	3.1	0.7	3.3	39
52	3-H	" "	65	-3			26
53	3-H	" " *	65	2			26
54	3-H	Nitrosopumilus maritimus		20	20.0		41
55	3-H	Sulfolobus solfataricus	85	0.2	0.2		39
56	rTCA	Aquifex aeolicus	85	5.4	5.4		39
57	rTCA	Chlorobium limicola	30	9.5	9.5		26
58	rTCA	Chlorobium phaeovibrioides*	30	10.4	10.0		26
59	rTCA	" " *	30	9.5			39
60	rTCA	Chlorobium thiosulfatophilum*	20	20.1	20.1		26
61	rTCA	Chlorobium vibrioforme*	30	12.2	11.3	0.7	26
62	rTCA	" "	30	10.8			39
63	rTCA	" "	30	10.7			26
64	rTCA	" "	28	11.4			26
65	rTCA	Chloroflexus aurantiacus	55	7.6	11.9	2.9	39
66	rTCA	" " *	55	13.7			39
67	rTCA	" "	55	12.7			26
68	rTCA	" "	55	13.6			26
69	rTCA	Desulfobacter hydrogenophilus	28	10	12.5	3.0	39
70	rTCA	" "	28	8.9			39
71	rTCA	" "	28	14.2			39
72	rTCA	" "	28	13.7			42
73	rTCA	" "	30	15.9			43
74	rTCA	Hydrogenobacter thermophilus	70	5.5	5.5		39
75	rTCA	Pyrobaculum aerophilum	100	2.9	2.9		39
76	rTCA	Thermocrinis ruber	85	3.3	3.3		26
77	rTCA	Thermoproteus neutrophilus	85	2	5.4		39
78	rTCA	" "		8.7			26
79	rTCA	Pyrodictium occultum	102	2.3	2.3		39

80	rTCA	Pyrolobus fumarii	105	3.8	3.8		39
81	rAP	Desulfotomaculum acetoxidans	30	30.5	29.5		42
82	rAP	" "	30	28.5			43
83	rAP	Desulfobacterium autotrophicum	28	39.3	24.3	16.7	26
84	rAP	" "	28	38.2			26
85	rAP	" "	30	10			42
86	rAP	" "		9.6			43
87	rAP	Archaeoglobus fulgidus	85	2.7	4.3		39
88	rAP	" "	85	5.8			39
89	rAP	Archaeoglobus lithotrophicus	85	8	8.0		39
90	rAP	Ferroglobus placidus	85	3.5	3.5		39
91	rAP	Acetobacterium woodii	28	22.2	22.3	6.6	26
92	rAP	" "	28	29			26
93	rAP	" "	28	15.8			26
94	rAP	M.bacterium thermoautotrophicum	65	12.7	25.9	9.9	44
95	rAP	" "	65	26.6			44
96	rAP	" "	65	43.8			44
97	rAP	" "	65	46			44
98	rAP	" "	65	24.5			44
99	rAP	" "	65	21.9			44
100	rAP	" "	65	23.1			44
101	rAP	" "	65	15			39
102	rAP	" "	65	19.1			26
103	rAP	" "	56	27			44
104	rAP	" "	56	26.6			44
105	rAP	" "	66	27.4			44
106	rAP	" "		34			44
107	rAP	" "	65	15			39
108	rAP	Methanobacterium formicicum	34	36.1	36.4	1.9	44
109	rAP	" "	34	38.4			44
110	rAP	" "	34	34.7			44
111	rAP	Methanobacterium sp.	37	25.1	22.9	2.8	26
112	rAP	" "	37	23.2			26
113	rAP	" "	46	18.8			26
114	rAP	" "	46	24.5			26
115	rAP	M.bacterium sp. strain Ivanov	37	25.2	22.8	3.0	44
116	rAP	" "	37	23.2			44
117	rAP	" "	46	18.5			44
118	rAP	" "	46	24.3			44
119	rAP	M.bacterium strain M.o.H.	40	11.5	11.5		44
120	rAP	M.caldococcus jannaschii	85	6.2	12.1	4.9	39
121	rAP	" "	85	17.7			39
122	rAP	" "	85	10.7			39

123	rAP	"	"	85	13.7			39
124	rAP	Methanococcus	igneus	85	20.2	21.5		39
125	rAP	M.coccus	thermolithotrophicus	65	22.7	18.6	7.6	39
126	rAP	"	"	65	25.8			39
127	rAP	"	"	65	26.7			39
128	rAP	"	"	41	7.4			39
129	rAP	"	"	51	13.5			39
130	rAP	"	"	60	19.7			39
131	rAP	"	"	65	24.8			39
132	rAP	"	"	65	26			39
133	rAP	"	"	70	24.9			39
134	rAP	"	"	65	8.7			39
135	rAP	"	"	45	20.5			39
136	rAP	"	"	45	13.4			39
137	rAP	"	"	45	4.8			39
138	rAP	"	"	65	22			39
139	rAP	Methanopyrus	kandleri	100	20.3	16.5		39
140	rAP	"	"	100	12.7			39
141	rAP	Methanosarcina	barkeri	37	19.5	16.3	2.3	39
142	rAP	"	"	40	14.8			44
143	rAP	"	"	37	14.6			44
144	rAP	"	"	37	16.3			44
145	rAP	Methanothermus	fervidus	85	13.1	13.1		39

Table S7. Mean $\delta^{13}\text{C}$ -isotopic fractionations from CO_2 to cell biomass ($\epsilon_{\text{CO}_2\text{-cells}}$) in microbes using the reductive acetyl CoA pathway, calculated from compiled data in Table S6.

Taxon	Energy metabolism	$\epsilon_{\text{CO}_2\text{-cells}}$ (‰)		Ref.
		mean	SD	
<i>Desulfotomaculum acetoxidans</i>	SO_4^{2-} reducer, H_2/CO_2	29.5		42-43 26,
<i>Desulfobacterium autotrophicum</i>	SO_4^{2-} reducer, H_2/CO_2	24.3	16.7	42-43
<i>Archaeoglobus fulgidus</i>	SO_4^{2-} reducer, H_2/CO_2	4.3		39
<i>Archaeoglobus lithotrophicus</i>	SO_4^{2-} reducer, H_2/CO_2	8.0		39
<i>Ferroglobus placidus</i>	Fe^{3+} , NO_3^- , $\text{S}_2\text{O}_3^{2-}$ reducer	3.5		39
<i>Acetobacterium woodii</i>	acetogenesis, H_2/CO_2	22.3	6.6	26, 42-43
<i>M.bacterium thermoautotrophicum</i>	methanogenesis, H_2/CO_2	25.9	9.9	26, 39, 44
<i>Methanobacterium formicicum</i>	methanogenesis, H_2/CO_2	36.4	1.9	44
<i>Methanobacterium</i> sp.	methanogenesis, H_2/CO_2	22.9	2.8	26
<i>Methanobacterium</i> sp. strain Ivanov	methanogenesis, H_2/CO_2	22.8	3.0	44
<i>Methanobacterium</i> strain M.o.H.	methanogenesis, H_2/CO_2	11.5		44
<i>Methanocaldococcus jannaschii</i>	methanogenesis, H_2/CO_2	12.1	4.9	39
<i>Methanococcus igneus</i>	methanogenesis, H_2/CO_2	21.5		39

Table S8. Media composition for initial enrichment and transfer. The composition, including the trace element and vitamin solutions, follows the methanogenic Medium 141 (DSMZ) except where indicated in bold. 2 atm headspace pressure of 80% H₂: 20% CO₂ were applied. The final pH was adjusted to 8.0. All incubations were at 65°C.

	Initial Enrichment	Transfer
Ingredients of Medium	Quantity L⁻¹	Quantity L⁻¹
KCl	0.34 g	0.34 g
MgCl ₂ x 6 H ₂ O	4.0 g	6.85 g
MgSO ₄ x 7 H ₂ O	3.45 g	omitted
NH ₄ Cl	0.25 g	0.25 g
CaCl ₂ x 2 H ₂ O	0.14 g	0.14 g
K ₂ HPO ₄	0.14 g	0.14 g
NaCl	18.0 g	18.0 g
Fe(NH ₄) ₂ (SO ₄) ₂ x 7 H ₂ O	2 mg	2 mg
NaHCO ₃	2.5 g (29.8 mM)	2.500 g (29.8 mM)
Na-acetate	0.082 g (1 mM)	0.164 g (2 mM)
Methanol stock (300 mM)	0.17 mL (50 μM)	1 mL (300 μM)
Dimethyl sulfide stock (30 mM)	1.67 mL (50 μM)	10 mL (300 μM)
Yeast extract (Difco)	0.20 g	0.200 g
Trypticase (BBL)	2.00 g	2.00 g
Resazurin	1 mg	1 mg
Cysteine-HCl x H ₂ O	0.50 g	0.50 g
Na ₂ S x 9 H ₂ O	0.50 g	0.50 g
Trace elements	10 mL	10 mL
Vitamin solution	10 mL	10 mL
Distilled water, added to:	1000 mL	1000 mL

Table S9. Basalt media composition after 7 years (initial) and 5 years (1st transfer) of incubation. bd = below detection; $\delta^{13}\text{C}$ -values in ‰ vs. VPDB.

Core ID	Replicate	enrichment	Aqueous concentrations				$\delta^{13}\text{C}$
			CH_4 (μM)	SO_4^{2-} (mM) ¹	H_2S (mM) ²	DIC (mM) ³	CH ₄ (‰)
1R-1-79	A	initial	0.0	17.0	bd	20.1	-62
1R-1-79	B	initial	0.0	17.3	bd	26.9	-64
14R-1-11	A	initial	0.1 ± 0.0	17.4	bd	27.4	-52
1R-1-79	A	1st transfer	0.7 ± 0.3	8.0	bd	1.4	-54
1R-1-79	B	1st transfer	1.6 ± 0.3	8.4	bd	2.4	-62 ⁴
14R-1-11	A	1st transfer	1.5	7.4	bd	2.2	-62 ⁴
23R-2-21	A	1st transfer	0.7 ± 0.5	7.7	bd	3.3	-65

¹⁾ initial concentration: 15.3 mM in original enrichment medium, 1.3 mM in transfer medium.

²⁾ initial concentration: 2.1 mM

³⁾ initial concentration: ≥ 29.8 mM

⁴⁾ average of duplicate measurements with precision of $\pm 1.5\%$.

Table S10. (A) Mean molar content of the potential electron donors Fe(II), S (AVS+CRS), and OC per liter of basalt. (B) Mean molar content of the potential electron acceptors Fe(III), SO₄, and IC per liter of basalt. All molar contents were calculated from mean weight percentages of Fe, S, and C fractions in host rock, and are from this study (Tables S2, S4, S13) except where indicated by footnotes. Molar contents of bulk data were converted from per gram to per liter assuming a basalt density of 2,750 g L⁻¹, which is the mean bulk density of basalt at U1301B (calculated from (9)). Molar contents of aqueous species (DOC, sulfate (*aq*), DIC) were calculated assuming a porosity of 5.3%, which is the mean porosity at U1301B (calculated from (9)), by multiplying mean concentrations from basement fluids sampled from boreholes or BBS by a factor of 0.053. These values are rough estimates since they assume that concentrations of basement fluids from boreholes or BBS fully reflect those within veins and basaltic pore space. CRS was assumed to be 100% pyrite (FeS₂). Abbreviations: FTT = Fischer-Tropsch-type, SR = sulfate reduction, MG = methanogenesis, AG = acetogenesis, Fe-red = Fe(III) reduction, FMT = fermentation, ND = not determined, N/A = not applicable (sample size < 3).

(A)

<i>e</i> ⁻ -donor	mol L ⁻¹ basalt		Potential energy-yielding reactions
	Mean	SD	
Fe(II) ¹	2.5E+00	2.5E-01	Indirect; biotic SR, MG, AG, Fe-red from (a) H ₂ produced by serpentinization and/or (b) small organic molecules produced by FTT synthesis
Olivine ^{1,2}	9.1E-01	1.2E+00	
S (AVS+CRS)	3.3E-02	2.7E-02	Indirect; biotic S ⁰ disproportionation of S species, e.g. produced by abiotic S ²⁻ oxidation with Fe(III)
AVS	7.1E-03	1.2E-02	
CRS	2.6E-02	2.3E-02	
TOC	6.2E-02	2.4E-02	Biotic SR, MG, AG; AOM, FMT
DOC ³	6.6E-7	N/A	Biotic SR, MG, AG; AOM, FMT

(B)

<i>e</i> ⁻ -acceptor	mol L ⁻¹ basalt		Potential energy-yielding reactions
	Mean	SD	
Fe(III) ¹	1.1E+00	3.7E-01	Abiotic Fe(III) reduction by reactions with S ²⁻ may restore bioavailable inorganic S species; biotic Fe-red
Sulfate (total)	9.5E-03	8.0E-03	Biotic SR, AOM
Sulfate (<i>aq</i>) ⁴	1.0E-03	N/A	Biotic SR, AOM
IC	ND	ND	Biotic MG, AG
DIC ⁵	2.0E-06	N/A	Biotic MG, AG

¹individual values (in wt %) shown in Table S11.

²averaged from 9.

³assumes 12.5 μM concentration, which is the average from 1026B and BBS (6).

⁴assumes 17.6 mM, which is value measured in U1301A borehole fluid (11).

⁵assumes 37.5 μM, which is the average from 1026B and BBS (10).

Table S11. Fe²⁺, Fe²⁺-olivine, Fe³⁺, and FeTotal (FeT) content in host rock and halos (halos in parentheses) at borehole U1301B. All data from this study, except Fe²⁺-olivine data, which was calculated from bulk olivine measurements published in reference 9.

Sample ID	Depth (mbsf)	weight %			
		Fe ²⁺	Fe ²⁺ - olivine	Fe ³⁺	FeT
1R-1-14	351.3		bd		
1R-1-79	352	4.8		3.5	8.3
1R-1-118	352.4		trace		
2R-1-4	357.1		0.7		
2R-2-98	359.6	5.4		2.3	7.7
4R-4-7	371.2	5.3		2.5	7.8
5R-1-22	377.5	5.4		1.9	7.4
6R-2-129	388.8	4.1 (5.1)		2.0 (4.5)	6.1 (9.6)
12R-1-31	429.2		5.5		
14R-1-11	434.1	5.6 (5.7)		1.7 (3.5)	7.3 (9.2)
15R-4-66	448.8		trace		
16R-1-83	454.0		2.2		
17R-1-70	462.1	4.4 (5.5)		2.2 (3.8)	6.5 (9.3)
18R-2-92	473.2		7.7		
19R-1-41	476.5	5.2 (5.1)		1.8 (3.7)	6.9 (8.9)
19R-1-132	477.4		1.7		
20R-1-57	481.2	5.0		3.7	8.7
21R-2-126	493.0		0.9		
23R-2-21	501.6	4.8 (5.9)		1.5 (1.8)	6.3 (7.8)
26R-1-41	515.9		1.1		
26R-1-76	516.3	5.8 (6.1)		1.5 (2.3)	7.3 (8.4)
35R-2-107	566.1		0.8		
36R-2-102	575.7		1.7		

Table S12. List of *dsrAB/dsrB* primers tested in study. *xdsrB* = xenologous *dsrB*, *rdsrB* = reverse *dsrB*.

Primer	Sequence (5' – 3')	Target groups	Reference
Dsr-1F	ACS CAC TGG AAG CAC G	General	14
Dsr-4R	GTG TAG CAG TTA CCG CA	General	14
Dsr 1F1	CAG GAY GAR CTK CAC CG	General	20
Dsr 1R1	CCC TGG GTR TGR AYR AT	General	20
Del1075R	GYT CVC GGT TCT TDC	δ Proteobacteria	45
Arch1830F	TGC TGT CNA ACA TG	<i>Archaeoglobales</i>	45
AG dsrF	GAG AGA GGA GCA ACR	<i>Archaeoglobales</i>	This study
AG-FC dsrR	TCG TCC CAC CAS TCC CA	<i>Archaeoglobales</i> , Firmicutes	This study
dsrB F1a	CAC ACC CAG GGC TGG	General except <i>xdsrB</i>	This study
dsrB F1b	CAT ACT CAG GGC TGG	General except <i>xdsrB</i>	This study
dsrB F1c	CAT ACC CAG GGC TGG	General except <i>xdsrB</i>	This study
dsrB F1d	CAC ACT CAA GGT TGG	General except <i>xdsrB</i>	This study
dsrB F1e	CAC ACA CAG GGA TGG	General except <i>xdsrB</i>	This study
dsrB F1f	CAC ACG CAG GGA TGG	General except <i>xdsrB</i>	This study
dsrB F1g	CAC ACG CAG GGG TGG	General except <i>xdsrB</i>	This study
dsrB F1h	CAT ACG CAA GGT TGG	General except <i>xdsrB</i>	This study
dsrB F2a	CGT CCA CAC CCA GGG	<i>xdsrB</i>	This study
dsrB F2b	TGT GCA TAC CCA GGG	<i>xdsrB</i>	This study
dsrB F2c	CAT TCA TAC CCA GGG	<i>xdsrB</i>	This study
dsrB F2d	TGT TCA CAC CCA GGG	<i>xdsrB</i>	This study
dsrB F2e	CGT GCA CAC GCA GGG	<i>xdsrB</i>	This study
dsrB F2f	CGT TCA TAC ACA GGG	<i>xdsrB</i>	This study
dsrB F2g	TGT CCA CAC TCA GGG	<i>xdsrB</i>	This study
dsrB F2h	CGT GCA TAC GCA GGG	<i>xdsrB</i>	This study
dsrB F2i	CAT CCA TAC TCA GGG	<i>xdsrB</i>	This study
dsrB 4RSI1a	CAG TTA CCG CAG TAC AT	General except <i>xdsrB</i> & <i>rdsrB</i>	This study
dsrB 4RSI1b	CAG TTA CCG CAG AAC AT	General except <i>rdsrB</i>	This study
dsrB 4RSI1c	CAG TTG CCG CAG TAC AT	General except <i>xdsrB</i> & <i>rdsrB</i>	This study
dsrB 4RSI1d	CAG TTT CCG CAG TAC AT	General except <i>xdsrB</i> & <i>rdsrB</i>	This study
dsrB 4RSI1e	CAG TTG CCG CAG AAC AT	General except <i>rdsrB</i>	This study
dsrB 4RSI1f	CAG TTT CCA CAG AAC AT	General except <i>xdsrB</i> & <i>rdsrB</i>	This study
dsrB 4RSI2a	CAG GCG CCG CAG CAG AT	<i>rdsrB</i>	This study
dsrB 4RSI2b	CAG GCG CCG CAG CAC AC	<i>rdsrB</i>	This study
dsrB 4RSI2c	CAT GCT CCG CAG CAG AT	<i>rdsrB</i>	This study
dsrB 4RSI2d	CAC GCG CCG CAA GCC AC	<i>rdsrB</i>	This study
dsrB 4RSI2e	CAT GCA CCA CAA CAA AT	<i>rdsrB</i>	This study
dsrB 4RSI2f	CAG GCA CCA CAG CAG AT	<i>rdsrB</i>	This study
dsrB 4RSI2g	CAG GCT CCG CAG CAG AT	<i>rdsrB</i>	This study
dsrB 4RSI2h	CAG GCG CCG CAG TAC AT	<i>rdsrB</i>	This study

Table S13. PCR primer combination, target group, fragment size, and DNA extracts tested. For pure cultures, 40 amplification cycles were used except where indicated. Since 4 of the original 10 sample DNA extracts from Hole U1301B had been used up for *mcrA* amplifications, only 6 DNA extracts could be checked for *dsr* presence. Due to low remaining volumes of DNA extract, we first amplified residual basalt DNA extracts with the DSR1F / 4R primer pair in a 50 μ L-PCR-reaction volume for 40 PCR cycles, and then used subsamples (2 μ L) for reamplifications in 40 cycles with the DSR1F / 4R primer pair, or nested PCR using other primer combinations. [*Dsv.* = *Desulfovibrio*, *Dsm.* = *Desulfotomaculum*, *Ag.* = *Archaeoglobus*.]

Primer Combination	Target Group	Size (bp)	Dsv. oceani	Dsm. spp. Eth ²	Ag. fulgidus*	Ag. sulfaticallidus ³	U1301 B
DSR1F / 4R	General	~1,900	+	+	+	-	-
Dsr-1F1 / -1R1	General	~1,000	+	+	nd	nd	-
DSR1F / Del1075R	δ Proteobacteria	~940	+	nd	nd	nd	-
Arch1830F / DSR4R	Archaeoglobales	~350	nd	nd	-	-	-
AG dsrF / DSR4R	Archaeoglobales	~1,100	nd	nd	+	-	-
Dsr-1F / AG-FC dsrR	Archaeoglobales,	~900	nd	nd	+	+	-
dsrB F1a-h / 4RSI1a-	General except	~350	- ¹	nd	+	+	+
dsrB F2a-i / 4RSI1b,e	xdsrB	~350	nd	+	nd	nd	-
dsrB F1a-h / 4RSI2a-	rdsrB	~350	nd	nd	nd	nd	-

¹ negative PCR result after 25 amplification cycles.

² Isolate provided by Flemming Mønsted Christensen.

³ Isolated from back rust deposit on borehole observatory at ODP Site 1026 (46). No published dsrAB sequence.